Simulating the role of biogeochemical hotspots in driving nitrogen export from dryland watersheds

[1]Jianning Ren, [1]Erin J. Hanan, [2]Aral Greene, [3]Christina Tague, [4]Alexander H. Krichels, [1]William D. Burke, [5]Joshua P. Schimel, [2]Peter M. Homyak

[1]Department of Natural Resources and Environmental Science, University of Nevada, Reno, 89501, Reno, USA

[2]Department of Environmental Sciences, University of California, Riverside, 92521, Riverside, USA

[3]Bren School of Environmental Science & Management, University of California, Santa Barbara, 93106, Santa Barbara, USA

[4]USDA Forest Service Rocky Mountain Research Station, 87102, Albuquerque, USA

[5]Department of Ecology, Evolution and Marine Biology, University of California, Santa Barbara, 93106, Santa Barbara, USA

Correspondence:

Jianning Ren (nren@unr.edu, renjianning@gmail.com)

Erin Hanan (ehanan@unr.edu)

Key Points:

- We developed a model framework to represent biogeochemical hotspots in dryland ecosystems.
- Nitrogen export is sensitive to parameters controlling hotspot abundance, subsurface hydrologic connectivity, and soil moisture dynamics.
- The abundance and physical characteristics of hotspots can affect the timing of hot moments.

Abstract

Climate change and nitrogen (N) pollution are altering biogeochemical and ecohydrological processes in dryland watersheds, increasing N export, and threatening water quality. While simulation models are useful for projecting how N export will change in the future, most models ignore biogeochemical "hotspots" that develop in drylands as moist microsites become hydrologically disconnected from plant roots when soils dry out. These hotspots enable N to accumulate over dry periods and rapidly flush to streams when soils wet up. To better project future N export, we developed a framework for representing hotspots using the ecohydrological model RHESSys. We then conducted a series of virtual experiments to understand how uncertainties in model structure and parameters influence N export. Modeled N export was sensitive to the abundance of hotspots in a watershed, increasing linearly and then reaching an asymptote with increasing hotspot abundance, which occurred because resource inputs eventually became limiting with increasing hotspot and decreasing vegetation cover. Peak streamflow N also increased and then decreased with an increasing soil moisture threshold required for subsurface flow from hotspots to reestablish. Finally, N export was generally higher when water diffused out of hotspots slowly because prolonged moisture availability enabled more N to accumulate over dry periods, which leached more rapidly at the onset of rain. In a case study, we found that when hotspots were modeled explicitly, peak streamflow nitrate export increased by 29%, enabling us to better capture the timing and magnitude of N losses observed in the field. N export further increased in response to interannual variability in precipitation, particularly when multiple dry years were followed by a wet year. This modeling framework can improve projections of N export in watersheds where hotspots play an increasingly important role in water quality.

1 Introduction

Climate change and atmospheric nitrogen (N) deposition from urbanization and fossil fuel combustion are accelerating biogeochemical cycling in dryland ecosystems and increasing N loading in streams, which can pose a major threat to water quality (Borer & Stevens, 2022; Fenn et al., 2003). However, the extent to which deposited N is exported to streams remains difficult to predict, in part because models are limited in their ability to capture hotspots—defined as wetter microsites in the soil that have disproportionately high rates of biogeochemical cycling—which can strongly influence N fluxes in dryland soils (McClain et al., 2003). For example, the already increased water availability and decreased plant N uptake in hotspots can increase net N mineralization and nitrification rates, enabling inorganic N to accumulate over relatively dry periods and rapidly flush to streams when soils wet up (McClain et al., 2003; Parker & Schimel, 2011). This can occur even when plants are N-limited because precipitation pulses can mobilize accumulated N more quickly than plants are able to take it up (Homyak et al., 2014). As the global distribution of drylands expands with climate warming (Seager et al., 2018), and as urbanization increases rates of N deposition (Borer & Stevens, 2022), it is critical to better account for the mechanisms driving N export in models (Gustine et al., 2022; Schimel, 2018).

Hotspots can range in size from microsites within soil aggregates (at the scale of microns; Ebrahimi & Or, 2018) to islands of fertility within landscape patches (at the scale of individual plants or plant communities; Osborne et al., 2020). While landscape models may effectively represent islands of fertility by parameterizing plant physiological processes that promote resource heterogeneity—for example, transpiration-driven nutrient accumulation beneath woody plant canopies in savannas; (Ridolfi et al., 2008)—representing the role of microscale biogeochemical hotspots is much more challenging at watershed scales. For one, soil moisture and subsurface transport processes are often oversimplified and not fully integrated into landscape-scale N-cycling models (Ouyang et al., 2017; Poblador et al., 2017; Schmidt et al., 2007; Zhang et al., 2018). When models do incorporate coupled hydrological-biogeochemical processes, they often reduce spatial heterogeneity by averaging soil hydraulic parameters across a basin (Crow et al., 2012; Lin et al., 2015; Tague, 2009; Zhu et al., 2012, 2015). As a result, these models do not capture the role of soil microsites that remain wetter than bulk soils for at least some time into the dry season. While more detailed representation of soil heterogeneity is needed, at least three key uncertainties remain in scaling microsite processes across an entire watershed: (1) how hotspots are distributed across watersheds (McClain et al., 2003) (2) the amount of precipitation required to reestablish hydrological connection between hotspots and bulk soils and to generate subsurface flow (Zhu et al., 2018), and (3) how the physical parameters governing fine-scale water diffusion from hotspots are distributed across a watershed (Clark et al., 2017).

A common modeling approach to represent the effects of fine-scale spatial heterogeneity on large-scale hydrologic fluxes is to incorporate distributions of sub-grid state variables that influence large-scale fluxes (i.e., statistical-dynamical flux parameterizations occurring within a grid cell; the smallest spatially explicit model unit; Clark et al., 2017; Wood et al., 1992). For example, Burke et al. (2021) developed an approach using the ecohydrological model RHESSys, which uses a distribution of aspatial, sub-grid vegetation patches that interact to influence grid-scale ecohydrological processes. For N-cycling, an approach that can represent microscale soil aggregates and their distinctive moisture, nitrogen and carbon availability can enable microscale hotspots function to be included in hillslope to watershed-scale models. By representing these microsites as 'aspatial' modeling units—where the exact location within a larger modeling unit—is unspecified, this approach can better capture spatial heterogeneity without requiring detailed spatial information at sub-grid scales or increasing computational costs. To better predict how climate change modifies N retention and export, we developed a framework for modeling belowground hotspots and their interactions with soil moisture and subsurface flow by expanding the Burke et al. (2021) aspatial approach. This new framework allows us to represent hotspots explicitly across the landscape and test uncertainties related to hotspots distribution and connectivity.

Our new modeling framework enables N to accumulate in microscale hotspots—represented aspatially within 10-meter resolution grid cells—which contain sufficient moisture for decomposition to occur but are hydrologically disconnected from roots when the soils dry out. These micro-scale hotspot patches slowly lose water through diffusion and evaporation over the course of the dry season and can become hydrologically reconnected to the surrounding vegetated patches when soils wet up. Using this framework, we conducted a set of virtual experiments in a dryland, chaparral watershed in southern California to characterize model sensitivity to three key sources of uncertainty: (1) the area percentage of hotspots within the watershed, (2) the length of time it takes for water to diffuse from hotspots during periods of drought, and (3) the moisture conditions under which hydrological connectivity between hotspot and non-hotspot locations reestablishes. Finally, we used field observations of N export to optimize the parameters controlling N dynamics and then with an optimized model, we investigated how precipitation patterns can influence hotspot effects on N export. This case study demonstrates how our modeling framework can be used to improve theoretical understanding of the role biogeochemical hotspots play in N cycling and retention in drylands.

2 Methods

2.1 Study area

Model simulations were conducted in the Bell 4 basin (0.14 km^2), which is part of the USDA Forest Service San Dimas Experimental Forest located northeast of Los Angeles, California (34°12′N, 117°47′E; Figure 1). Elevations in Bell 4 range from 700 to 1024 meters. The topography is characterized by steep slopes with steep channel gradients. Soils are shallow, coarse-textured sandy loams, which are weathered from granite (Chaney et al., 2016; Dunn et al., 1988) and classified as Typic Xerorthents (Soil Survey Staff, 2022). The region has hot, dry summers (June to September around 14±18 mm precipitation, daily average temperature 23±4 °C) and cool, moist winters (696±380 mm precipitation, daily average temperature 14±5 °C); mean annual precipitation is around 710±402 mm. Vegetation cover is mainly mixed chaparral with chamise (*Adenostoma fasciculatum*), ceanothus (*Ceanothus spp*.), and black sage (*Salvia mellifera*) on south-facing slopes; ceanothus and California laurel (*Umbellularia californica)* on north-facing slopes; and some live oak (*Quercus agrifolia*) along riparian areas (Wohlgemuth, 2006).

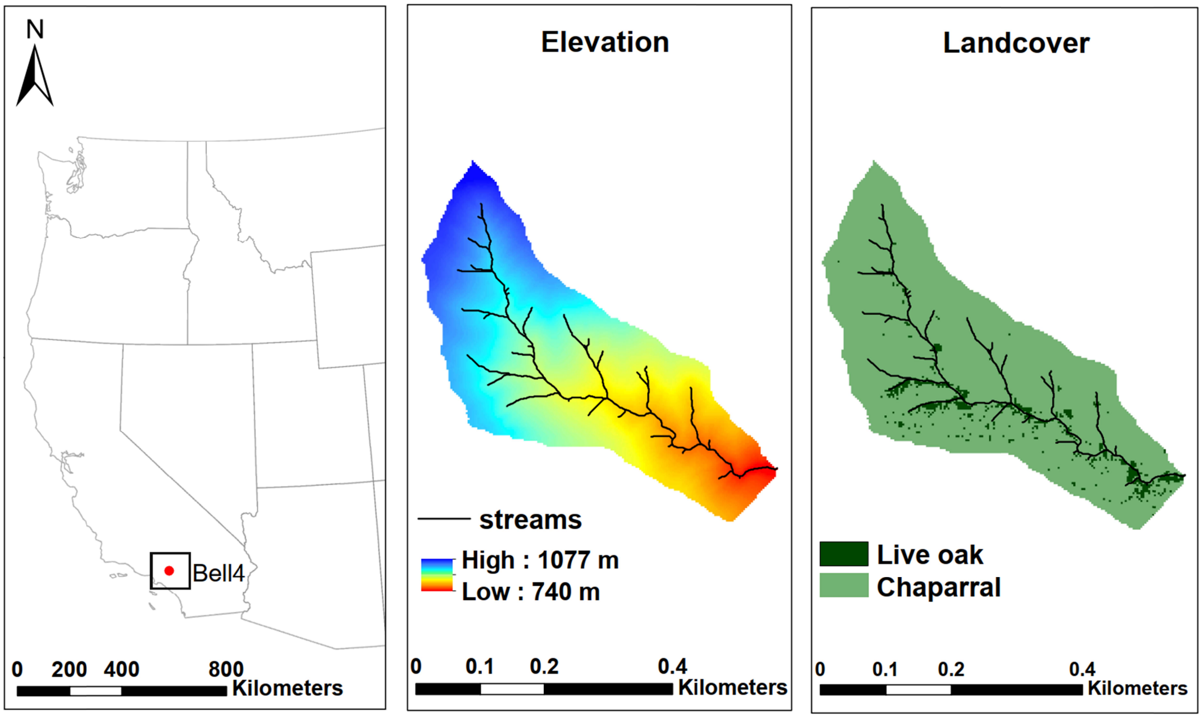

Figure 1. Bell 4 watershed in the USDA Forest Service San Dims Experimental Forest located in southern California, U.S. (34°12´N, 117°47´E). The watershed is 0.14 km^2.

2.2 RHESSys model

The regional hydro-ecologic simulation system (RHESSys) is a spatially distributed, process-based model that simulates interacting ecohydrological and biogeochemical processes at multiple scales (Chen et al., 2020; Hanan et al., 2017; Tague, 2009; Tague & Band, 2004). The smallest spatial unit is the "patch," which has a 10-meter resolution in the current study. At the patch scale, vertical hydrologic fluxes include canopy interception, transpiration, evaporation, infiltration, capillary rise, and drainage from the rooting zone to the saturated zone. Carbon (C) cycling processes are tightly coupled with hydrology and soil moisture and include photosynthesis, allocation of net photosynthate, plant and soil respiration, and litter and soil decomposition. Nitrogen cycling includes atmospheric N deposition, mineralization, nitrification, immobilization, denitrification, plant uptake, and export to streams (Figure 2, Hanan et al., 2017;

Lin et al., 2015). RHESSys has been parameterized and validated in several watersheds across the western USA (Burke et al., 2021; Garcia et al., 2016; Ren et al., 2021, 2022; Tague, 2009), including in several chaparral watersheds (e.g., Chen et al., 2020; Hanan et al., 2017, 2021; Meentemeyer & Moody, 2002).

There are four layers for vertical soil moisture processes, including a surface detention store, a root zone store, an unsaturated store below the root zone, and a saturated store. The vertical hydrologic processes also include canopy layers, snowpack, and litter moisture stores. Rain throughfall from multiple canopy layers and a litter layer provide potential infiltration. Then the surface detention storage receives water from canopy throughfall and snowmelt at a daily time step. Following precipitation and throughfall, water infiltrates into the soil following the Phillip (1957) infiltration equation. At a daily timestep, ponded water that has not infiltrated is added to detention storage and any water that is above detention storage capacity generates overland flow.

Infiltration updates one of three possible stores: a saturated store when the water table reaches the surface, a rooting zone store, or an unsaturated store for unvegetated patches. A portion of infiltrated water can bypass the rooting zone and unsaturated store through macropores. This bypass flow (carrying N) is added to a deeper groundwater store at the subbasin scale (Figure 2). Water drains vertically from the unsaturated store or root zone store based on hydraulic conductivity. Capillary rise moves water from the saturated zone to the root zone or unsaturated store based on Eagleson (1978). Lateral fluxes can occur through both shallow subsurface flow between patches and through bypass flow that contributes to a deeper hillslope-scale groundwater flow model. Shallow subsurface saturated flow between patches follows topography and changes with saturation deficit and transmissivity.

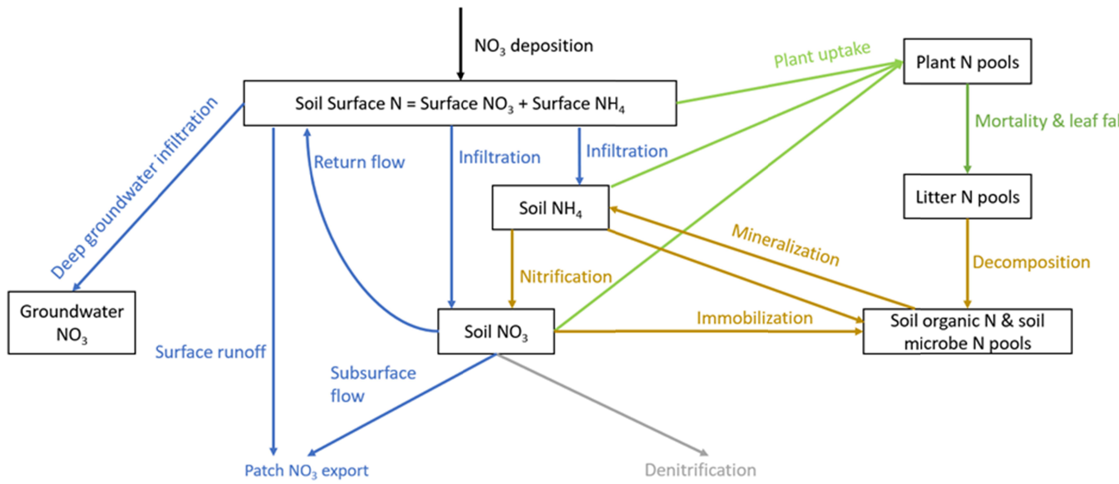

Figure 2. Conceptual diagram of nitrogen pathways in RHESSys, modified from Lin et al. (2015)

Hydrologic fluxes interact with several vegetation and soil parameters to influence biogeochemical cycling. RHESSys has four litter and four soil pools with varying C:N ratios and decomposition rates. Litter pools have two types of inputs: (1) leaves and coarse wood debris from aboveground vegetation and (2) fine root turnover. Decomposition is calculated as a defined maximum decomposition rate that is modified by soil moisture, soil temperature, nitrogen availability. Higher organic matter and lower leaf and litter C:N ratios increase decomposition rates. N mineralization and immobilization are calculated based on the C:N ratios of the litter and soil pools where C and N are being transferred (e.g., litter 1 to soil 1; Hanan et al., 2017; Tague & Band, 2004).

Nitrification rates in RHESSys are calculated based on the CENTURY$_{NGAS}$ model, where the nitrification rate is a function of soil pH (f_{pH}; Hanan et al 2017), moisture (f_{H_2O}), soil temperature (f_T), and available soil ammonium (f_{NH_4}; Parton, 1996):

$$N_{nitrif} = soil.NH4 \times f_{pH} \times f_{H_2O} \times f_T \times f_{NH_4} \qquad \text{Eq (1)}$$

The pH scalar (f_{pH}) is calculated as:

$$f_{pH} = \frac{0.56 + arctan(\pi \times 0.45 \times (-5 + pH))}{\pi} \quad \text{Eq (2)}$$

The soil moisture scalar (f_{H_2O}) is calculated as:

$$f_{H_2O} = (\frac{\theta - b}{a - b})^{d(\frac{b-a}{a-c})} (\frac{\theta - c}{a - c})^{d} \quad \text{Eq (3)}$$

where *a*, *b*, *c*, and *d* are parameters related to soil texture based on Parton et al. (1996) and θ is volumetric soil moisture.

The temperature scalar (f_T) is calculated as:

$$f_T = 0.06 + 0.13exp^{0.07T_{soil}} \quad \text{Eq (4)}$$

where T_{soil} is the surface soil temperature in degrees C.

The ammonium concentration available for nitrification is calculated as:

$$f_{NH_4} = 1.0 - \ exp^{[-0.0105 * NH_{4conc}]} \quad \text{Eq (5)}$$

where NH_{4conc} is the soil ammonium concentration in the fast-cycling soil layer.

N loss includes subsurface lateral flow of ammonium, nitrate, and dissolved organic N (DON) and denitrification. Denitrification is calculated based on a maximum denitrification rate (R_{NO_3}), and is modified by soil moisture (f_{H_2O}), and soil respiration (f_{hrCO_2}):

$$N_{denitrif} = R_{NO_3} \times f_{H_2O} \times f_{hrCO_2} \quad \text{Eq (6)}$$

The maximum denitrification rate is calculated as:

$$R_{NO3} = 0.0011 + \frac{a\ tan(\pi \times 0.002 \times \left(\frac{NO_{3\_soil}}{N_{soil} + C_{soil}} - 180\right))}{\pi} \quad \text{Eq (7)}$$

where NO_{3_soil} is the available nitrate (kg N m^{-2}) in soil and N_{soil} and C_{soil} are soil N (kg N m^{-2}) and C (kg C m^{-2}) amounts, respectively.

The soil moisture limitation is calculated as:

$$f_{H_2O} = \frac{a}{b^{\left(\frac{c}{b^{d \times \theta}}\right)}} \qquad \text{Eq (8)}$$

θ, a, b, c, and d are defined in Eq 3 above.

The effect of soil respiration is calculated as:

$$f_{hrCO_2} = \frac{0.0024}{1 + \frac{200}{e^{(3.5 \times hr)}}} - 0.00001 \qquad \text{Eq (9)}$$

where hr is total daily respiration (g N m^{-2} day^{-1}).

Nitrate enters the soil through infiltration from the surface detention store. Nitrate in the soil is transported by subsurface flow in the saturated zone, while in the unsaturated soil, there is no lateral nitrate transport (Chen et al., 2020; Tague & Band, 2004). The amount of nitrate in the unsaturated soil, including root accessible unsaturated soil, is maintained through the balance of input processes (nitrification and N-deposition) and loss through plant-uptake, denitrification, and export. The vertical distribution of current soil nitrate within the unsaturated zone determines the proportion that is flushed by rising water tables (saturated zone water). The vertical distribution of nitrate in the soil profile of the unsaturated zone is assumed to follow an exponential decay function, where the surface layer has more nitrate and deeper soil has less. The available nitrate at soil depth z is calculated as:

$$NO_{3\_soil}(z) = NO_{3\_surface} \times exp^{-N_{decay} \times z} \qquad \text{Eq (10)}$$

where $NO_{3\_surface}$ is nitrate at soil surface and N_{decay} is a soil specific parameter that defines the rate of nitrate decay. When water is moving between the unsaturated zone and the saturated zone, through downward leaching or upward capillary rise, nitrate moves with water based on its concentration.

Nitrate export follows the flushing hypothesis (Chen et al., 2020). As the water table rises, more N becomes available for flushing. The total soil nitrate export (NO_{3_out}) is calculated as the integration of soil nitrate below the water table:

$$NO_{3\_out} = \int_{z_{max}}^{z_s} \frac{q_z}{S_z} NO_{3\_soil} NO_{3\_mobile} \qquad \text{Eq (11)}$$

where z_{max} is the maximum water table depth, z_s is current water table depth, q_z is the net lateral transport of water from the patch at depth Z; S_z is the soil water content (in meters) and NO_{3_mobile} is a parameter that defines the portion of nitrate that is mobile (related to soil type). For example, sandy soils have lower surface area available for cation retention than finer soils, therefore causing higher NO_3^- mobility (Hallaq, 2010; Hassink, 1994; Witheetrirong et al., 2011). Mobile surface N can also be transported to deep groundwater through preferential flow paths.

Recent improvements to RHESSys enable users to account for fine-scale (within patch) heterogeneity (e.g., different types of vegetation cover and associated soil layers that may share water within a single patch; see Burke et al. 2021 for details). These are referred to as "aspatial patches." When running RHESSys using the aspatial patch framework, “patch families” become the smallest spatially explicit model unit, and aspatial patches (nested within a patch family) are the smallest aspatial model unit. Note that an aspatial patch within a patch family is used to represent a distribution of a given vegetation type (e.g., trees or shrubs) based on observed (or hypothetical) distributions. It can, but does not necessarily, represent a single stand or clump of vegetation cover; vegetation from a single aspatial patch within a patch family does not have a defined distribution in RHESSys, so the assumption is that biophysical interactions, such as the extent to which a given cover type shares water, are more important than their physical location within the finest grid cell. Because there are no physical locations of aspatial patches within a patch family, within patch heterogeneity can be modeled without explicitly parameterizing and modeling fine scale spatial units that would be both computationally prohibitive and nearly impossible to parameterize with measured data.

Local water routing between aspatial patches inside a patch family is based on root access to shared storages of water (Figure 3). Local routing allocates water between aspatial patches based on user defined rules. Local routing within the patch family occurs in addition to traditional hillslope routing which moves water laterally based on elevation gradients. Most commonly, water is distributed among aspatial patches as a function of relative differences between their rooting and unsaturated zone water contents and mediated by gaining and losing coefficients defined for each cover type.

In this framework, an aspatial patch will gain water if its water content is below the patch family mean and will lose water if it is above the mean, with the rate of water transfer controlled by sharing coefficients: loss coefficients (sh_l) and gain coefficients (sh_g). sh_l multiplies the water fluxes out of a patch and sh_g multiplies the water fluxes into a patch. Sharing coefficients are used to capture the integrated effects of uncertain, fine-scale variation in root distributions, and how root distributions and forest structure interact with fine-scale soil drainage characteristics. Nitrate and dissolved organic C are exchanged along with water during local routing.

2.3 Model development

To enable RHESSys to account for biogeochemical hotspots, we expanded the aspatial patch framework to incorporate "hotspot" aspatial patches within each patch family. These hotspot aspatial patches represent a distribution of unvegetated microsites where biogeochemical cycling can be hydrologically disconnected, as soils dry out, from aspatial patches that contain plant roots (Figure 3). To model hotspot aspatial patches (hereafter called hotspots), we implemented three key model developments: (1) model algorithms that enable hotspots to access soil and litter C and N from neighboring non-hotspot patches for decomposition and biogeochemical cycling, and (2) algorithms and parameters that control the moisture conditions under which hotspots are hydrologically disconnected from other aspatial patches in the saturated zone, (3) parameters that control water diffusion in the unsaturated and/or root zone between hotspot and non-hotspot patches as soils dry out.

Research has shown that N-rich microsites can occur in unvegetated locations where there is less N uptake and less water demand from plants (Zhu et al., 2018). In the original RHESSys framework, unvegetated patches were used to represent large (e.g., 10 to 30-meter resolution) areas with no vegetation. Without vegetation inputs, these patches did not develop C and N stores to support microbial biogeochemical cycling. To generate hotspots, we implemented a litter sharing scheme that moves litter from vegetated aspatial patches to hotspots at an annual timestep to coincide with litter fall (Figure 3). Because we assume that hotspot aspatial patches occur at fine scales across a given 10-meter resolution patch family, it is reasonable to assume that they have access to plant litter for decomposition and N cycling from other aspatial patches within the patch family. The amount of litter shared (CN_{share}) is a function of the mean litter C and N content of the patch family (CN_{mean}), where the amount of C and N in a hotspot patch after litter sharing (*$CN_{hotspot}$*) cannot be above the patch family mean (Eq 12). To enable N cycling in hotspots, hotspots also have access to 1% of the slow cycling (i.e., protected or passive) soil organic C and N pools from the vegetated patch families. The litter C and N routing is described as

$$CN_{share} = \frac{(\sum_{i=1}^{n_{veg}} (CN_{veg\_i} - CN_{mean}) \times coef\_litter)}{n_{hotspot}} \qquad \text{Eq (12)}$$

$$CN_{hotspot\_after} = min(CN_{hotspot\_before} + CN_{share} \, , \, CN_{mean}) \qquad \text{Eq (13)}$$

$$CN_{veg\_after\_i} = CN_{veg\_i} - \left(CN_{veg\_i} - CN_{mean}\right) \times coef\_litter \qquad \text{Eq (14)}$$

where, n_{veg} is the number of non-hotspot patches in a patch family, CN_{veg} is the amount of litter C and N in a non-hotspot patch, $n_{hotspot}$ is the number of hotspot patches in a patch family. *Coef_litter* is the sharing coefficient parameter that controls the amount of litter sharing. Hotspot patches can also be assigned a finer soil texture (e.g., loam), which can hold more water than non-hotspot patches. In the current model, non-hotspot patches were comprised of sandy loam (based on the POLARIS database; Chaney et al., 2016).

To control subsurface hydrologic flow from hotspots to vegetated patches, we set up a soil moisture threshold for non-hotspot patches (θ_{th}), above which, water flows into them from the saturated zone in hotspots. In other words, when non-hotspot patches dry down, they become hydrologically disconnected from hotspots and they become reconnected when soils wet up (Figure 3c & Eq 15).

$$\begin{cases} \theta_{veg} > \theta_{th}: \ water\ and\ nitrate\ leaching\ from\ hotspots\ to\ neighboring\ non-hotspot\ patches \\ \theta_{veg} \le \theta_{th}: \ no\ subsurface\ flow\ from\ hotspots\ to\ neighboring\ non-hotspot\ patches \end{cases} \quad \boldsymbol{Eq\ (15)}$$

where θ_{veg} is the soil moisture in non-hotspot patches.

This threshold is used to define a condition where "water films" can form as soils dry down, which enables microscale biogeochemical cycling while reducing nitrate leaching from hotspots over the course of the hot, dry summer (Parker & Schimel, 2011). When soils rewet at the onset of the rainy season, the water table rises, and hydrologic connectivity reestablishes between hotspot and non-hotspot patches. This can lead to rapid nitrification and nitrate export before plants become active and gain access to N that accumulated during dry periods of hydrologic disconnection (Parker & Schimel, 2011). While the thresholds at which hydrologic connectivity reestablishes are not currently well established, the threshold parameter can be calibrated to match field observations.

Although subsurface flow from hotspot patches remains somewhat disconnected during the dry season, water can still slowly diffuse from hotspots as soils dry out. To account for this, we developed water sharing coefficients that constrain local routing to and from hotspots and the unsaturated and rooting zone in the surrounding non-hotspot patches (Figure 3a). During the dry season (June to November), the default *sh_g* was set to 0.05 and *sh_l* was set to 0.9 to simulate hotspots losing water. During the wet season (December to May), the default *sh_g* was 0.9 and *sh_l* was 0.05 to simulate hotspots gaining water. We rely on sharing coefficients here to capture "film" dynamics that depend on micro-scale characteristics that are not feasible to explicitly model but have been documented to influence hot-spot dynamics in field and lab-studies (Homyak et al., 2016; Parker & Schimel, 2011). To summarize, while soil moisture gradients control whether routing occurs in the saturated zone between hotspot and non-hotspot patches, the sharing coefficients control the rate of local water transfer in the unsaturated zone.

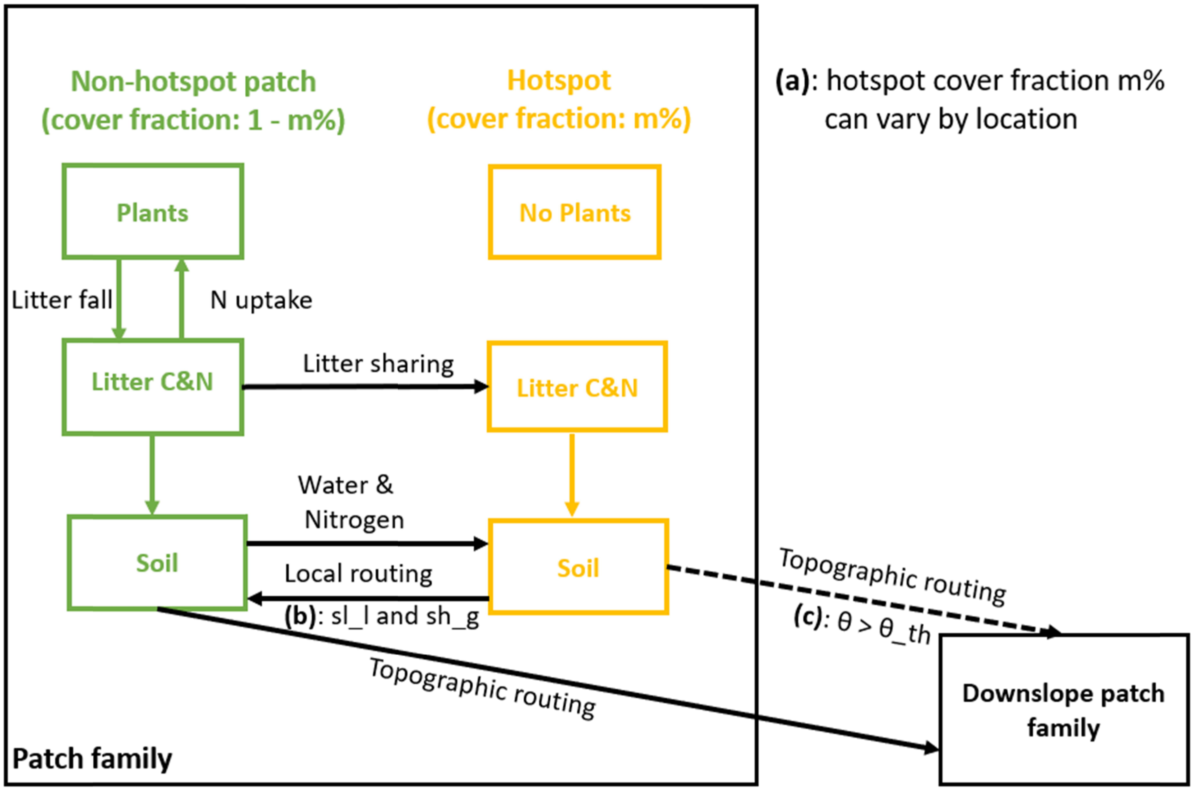

Figure 3. Conceptual overview of hotspots patches nested within each patch family. Each year, vegetated patches share litter C and N with hotspot patches from the portions of their stores that are greater than the patch family means. Note that the conceptual figure does not indicate that there is only one hotpot and one non-hotspot patch in a patch family, but rather represents their cover fraction. Key model uncertainties include: (a) hotspot cover fraction m%, which can vary by location, (b) local routing of water and N in the unsaturated zone between aspatial patches based on the mean water content of the patch family, which can be mediated by sharing coefficients sh_l and sh_g; and (c) topographic routing in the saturated zone from patches in one patch family to patches in downslope patch families, which can be controlled by a soil moisture threshold θ_{th}*. The dashed lines signify that hotspots are hydrologically disconnected from non-hotspot patches during dry periods but reconnect during wet periods when soil moisture in non-hotspot patch is larger than* θ_{th}*. The extent of hydrological routing between hotspot and non-hotspot patches is controlled by* θ_{th}*, which can be calibrated to match field observations.*

2.4 Data

To generate metrological inputs for RHESSys scenarios in Bell 4 using the new hotspot framework, we compared daily meteorological data from gridMET (Abatzoglou, 2013), including maximum and minimum temperatures, precipitation, relative humidity, radiation, and wind speed, from 1979 to 2020, to daily meteorological data at a station located near Bell 4 (San

Dimas Tanbark) from the USDA Forest Service (USFS). Because gridMET matched closely with ground station data but does not require gap filling, gridMET was selected as a suitable meteorological forcing dataset for our analyses. To calibrate drainage parameters, we used streamflow data from the USFS for the years 1980 to 2002; data were missing for some months (Figure 4). Because vegetation has different growth and transpiration rates after fire, which leads to a non-steady steady state conditions, we omitted 8 years of streamflow data (1984-1992) following a prescribed fire that occurred in 1984 (Meixner et al., 2006). We selected streamflow data from 1993 to 2002 for model calibration and 1980 to 1983 for validation (described in section 2.5 below).

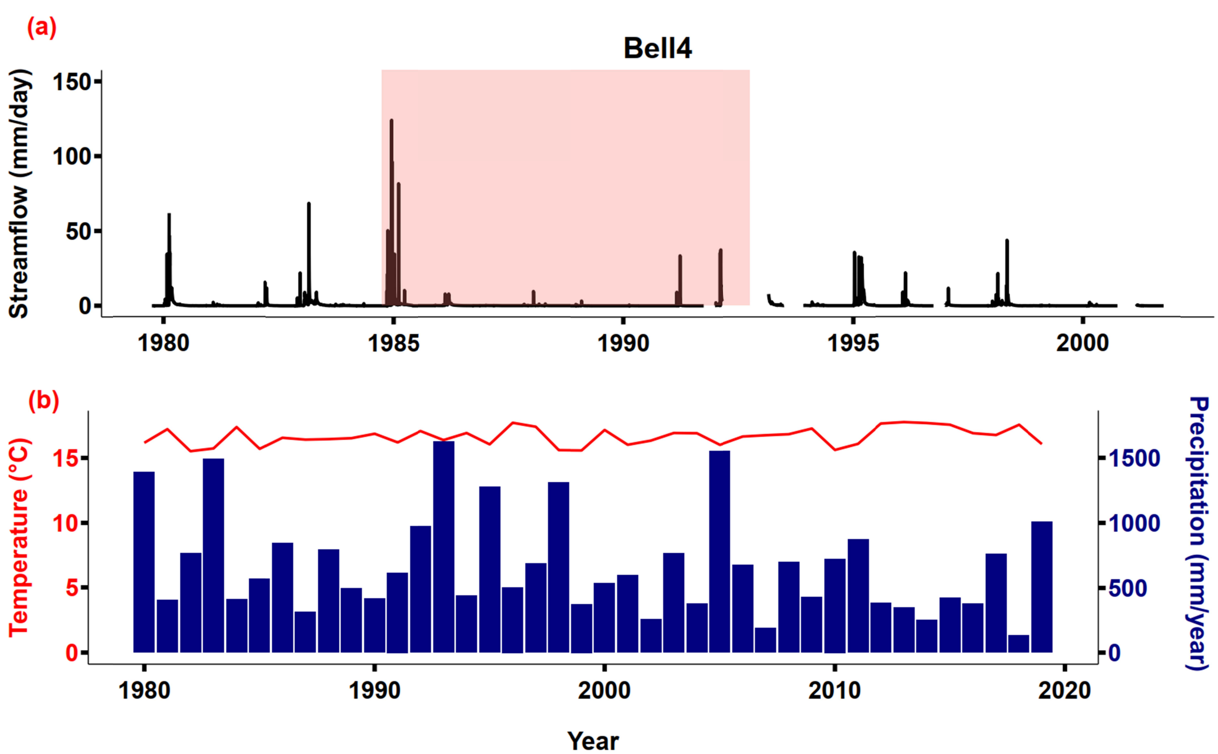

Figure 4. Streamflow and climate data for Bell 4. The temperature is yearly average, and streamflow is calculated as the volume divided by the catchment area (0.14 km^2). The red shaded period of streamflow data followed a large fire and was therefore not used for calibration.

We used a 10-meter resolution Digital Elevation Model (DEM, aggregated from 1-meter resolution LiDAR) to delineate slope, aspect, and wetness index at the patch family scale across the watershed. Aspatial patches are situated within the 10-meter resolution patch family and include both vegetated areas and soil aggregates that are isolated from plant roots and may serve as potential hots spots. In total we delineated 1259 10-meter resolution patch families for Bell 4. To map landcover, we aggregated 1-meter resolution land cover data from the National Agriculture Imagery Program (NAIP; collected on June 5, 2016) to 3-meter and classified three land cover types: chaparral, live oak, and bare ground (Maxwell et al., 2017). We then overlapped the 10-meter resolution DEM with 3-meter vegetation cover data to classify aspatial patch distributions in each patch family using a k-means function (Hartigan & Wong, 1979) in R version 4.3.0 (R Core Team, 2022). This resulted in approximately 11 aspatial patches in each patch family and 375 different vegetation combinations across the watershed. In total, there were 13716 aspatial patches for Bell 4. We acquired soil texture data from POLARIS (Chaney et al., 2016).

2.5 Model initialization, calibration, and evaluation

We initialized the soil C and N pools by running the model until the pools stabilized. For the vegetation C and N pools, we used a target-driven method that allows vegetation in each patch family to grow until it reaches target leaf area index (LAI) values from remote sensing data (Hanan et al., 2018). This method enables C and N pools to spin up mechanistically while still capturing landscape heterogeneity resulting from local resource limitations and disturbance histories. To construct a map of target LAI values, we chose the clearest available NAIP image during the growing season (i.e., April 24, 2010). We then calculated NDVI using Eq 16.

$$NDVI = \frac{\rho_{NIR} - \rho_R}{\rho_{NIR} + \rho_R} \quad \text{Eq (16)}$$

In this equation, ρ_{NIR} is the reflectance in the near-infrared, and ρ_R is reflectance in the red (Hanan et al., 2018). We then estimated LAI using a generalized NDVI-LAI model developed by (Baret et al. 1989; Eq 17).

$$LAI = -\frac{1}{k} \times ln(\frac{NDVI_{max} - NDVI}{NDVI_{max} - NDVI_{back}}) \qquad \text{Eq (17)}$$

Here, k is the extinction of solar radiation through a canopy. $NDVI_{max}$ is the maximum NDVI occurring in the region, and $NDVI_{back}$ is the background NDVI (i.e., from pixels without vegetation). When NDVI is equal to $NDVI_{max}$ we assign the infinite LAI value as the maximum observed LAI in this region based on literature (Garson & Lacaze, 2003; McMichael et al., 2004). We obtained k value from Smith et al. (1991) and White et al. (2000). The other parameters were obtained for each vegetation type (Table 1).

Table 1. Parameters used for calculating LAI from NDVI

Vegetation type	k	$NDVI_{max}$	$NDVI_{back}$
Live oak	0.500	0.379	-0.160
Chaparral	0.371	0.372	-0.160

We used observed streamflow for Bell 4 to calibrate six soil parameters: saturated hydraulic conductivity (K_{sat}), the decay of K_{sat} with depth (m), pore size index (b), air entry pressure (ϕ), bypass flow to deeper groundwater storage (gw_1), and deep groundwater drainage rates to stream (gw_2). We selected the best parameter set by comparing observed and modeled streamflow using monthly Nash-Sutcliffe efficiency (NSE; Nash & Sutcliffe, 1970) and percent error in annual flow estimates. NSE is used to evaluate peak flows and can range from -∞ to 1, where 1 represents a perfect fit between modeled and observed data. Percent error is used to compare differences between the total quantity of modeled and observed streamflow; values closer to zero represent better fit.

2.6 Sensitivity analyses and simulation scenarios:

After model initialization and calibration, we used the new model framework to build in microscale hotspots. We assumed the hotspots were evenly distributed across the landscape and converted one bare ground patch inside of every patch family to an aspatial hotspot patch. Note that this does not mean that there was only one hotspot in a patch family, but one aspatial patch was used to represent the distribution (or percent cover) of microscale hotspots. If no bare ground patches existed in the patch family, we instead converted a chaparral patch to an aspatial hotspot patch. Because there were approximately 11 patches in each patch family, this setup resulted in approximately 9% of each patch family (and of the overall basin) consisting of microscale hotspots. We also assigned a loam soil texture to hotspot patches to represent the soil physical properties that may also increase moisture retention. The default parameters used to represent hotspot hydrological and biogeochemical dynamics are shown in Table 2.

Table 2. Default parameters for hotspots. Sh_l and sh_g control water diffusion in the unsaturated zone between hotspot and non-hotspot patches, the default values promote strong seasonality in hotspot soil moisture. The soil moisture threshold controls water flow in the saturated zone between hotspot and non-hotspot patches; the default value promotes the maximum peak streamflow N. We defined one aspatial patch as a hotspot inside of each family. This leads to 9.1% cover of hotspot patches evenly distributed across the landscape.

Parameters	Value
Sharing coefficient of losing water in unsaturated zone from hotspots (sh_l)	Dry season: 0.9 Wet season: 0.05
Sharing coefficient of gaining water in unsaturated zone of hotspots (sh_g)	Dry season: 0.05 Wet season: 0.9
Soil moisture threshold of non-hotspot above which water in saturated zone flows from hotspots to non-hotspot (θ_{th})	21%
Percentage cover of hotspots	9.1%

Sharing coefficient of litter from non-hotspot patches to hotspot patches (coef_litter)	1

To evaluate the uncertainties related to model structure and parameters, we conducted a set of virtual experiments, or sensitivity analyses. For each sensitivity analysis, we ran RHESSys for 60 years by looping the available climate data from 1979-2020. Results are presented as simulation years and capture the climate variability from the available record. First, we examined how the percentage cover of hotspots can influence N export. We built hotspot patches from zero percent to 13.7 percent at 2.3 percent increments (i.e., 0%, 2.2%, 4.5%, 6.8%, 9.1%, 11.4%, 13.7%). When the hotspot percentage was equal to 9.1%, there were exactly one aspatial hotspot patch in each patch family. When the hotspot percentage was larger than 9.1%, we needed to convert two aspatial patches in some patch families to hotspot patches. For example, the scenario with 11.4% hotspot cover at the watershed scale, required 2.3% of patch families to have two aspatial hotspot patches. We emphasize this does not mean that there were only one or two hotspots in a patch family, but one or two aspatial patches were used to represent their distribution.

Second, we investigated how the saturation status of hotspots influences nitrate export. We built three soil moisture conditions for hotspots by changing the sharing coefficients for local routing, which influenced connectivity between hotspot and surrounding patches (Figure 3b): wet (sh_l was 0.05 and sh_g was 0.9 throughout the year; water diffused slowly from hotspots), dry (sh_l and sh_g were set to default values, hotspots diffused water quickly during the dry season), and intermediately-moist (sh_l was 0.1 and sh_g was 0.8 during the dry season but used default values in the wet season; water diffused from hotspots at an intermediate rate). The hotspots in the wet scenario were saturated almost all the time and had small interannual variation in soil moisture. The hotspots in the dry scenario lost water during dry periods and had large interannual soil moisture variation. The hotspots in the intermediately-moist scenario had soil moisture dynamics in between the levels observed in the dry and wet scenarios (Figure 5).

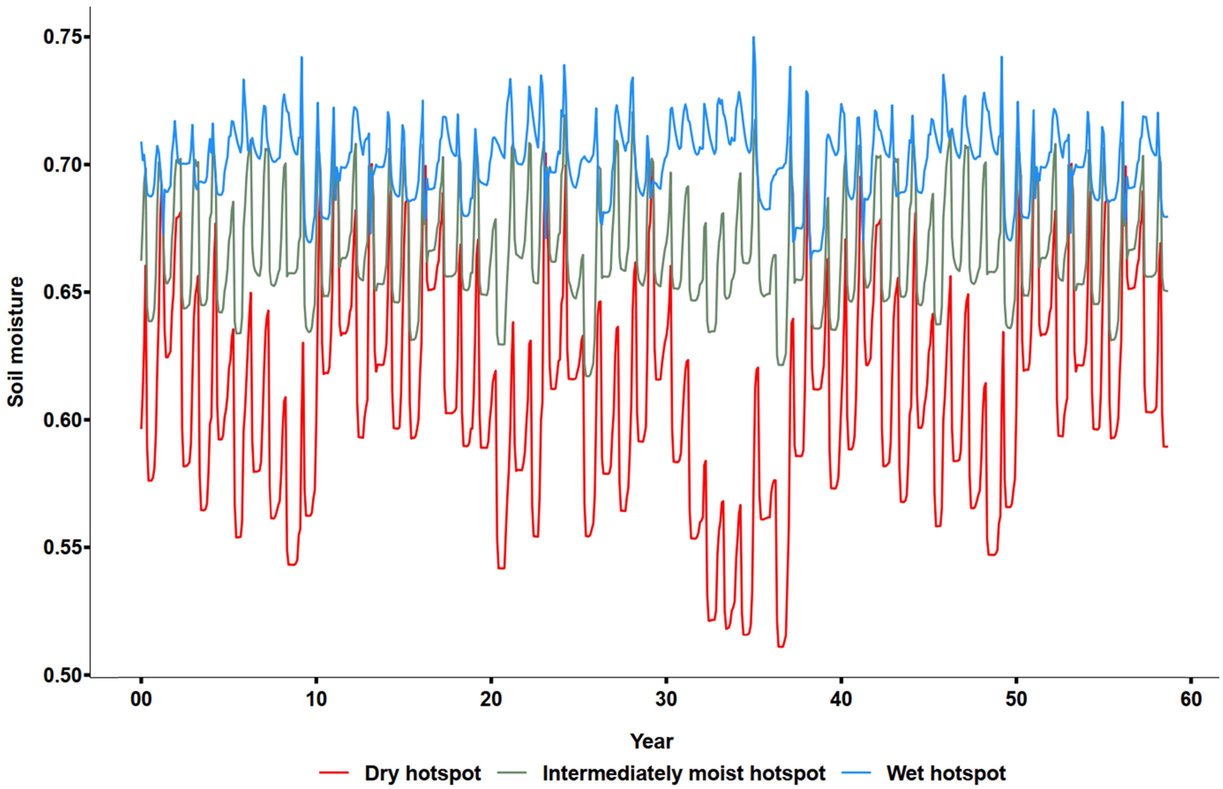

Figure 5. Hotspot volumetric soil moisture (unitless, in the scale of 0 to 1) conditions used to examine the sensitivity of N cycling and export to hotspot soil moisture saturation status and timing.

Lastly, we examined how uncertainty in the subsurface connectivity threshold parameter, which determines when non-hotspot patches become reconnected and can receive substantial N and water from the hotspot (θ_{th}; Figure 3c). By establishing conditions for this larger scale connectivity, this parameter can influence streamflow nitrate export. We then compared modeled streamflow nitrate export (under a range of parameter values based on the range of basin scale soil moisture: 0.15, 0.21, 0.25, 0.31, 0.35) to observed data (from 1988 to 2001).

Following the sensitivity analyses, we used available data and literature to estimate the most likely value for these parameters. We selected hotspot abundance of 9.1% assuming every patch family had the same hotspot coverage (using the default value in Table 2). We then selected the "dry" hotspot scenario in order to most closely match the seasonality of N dynamics observed in dryland ecosystems (Parker & Schimel 2011). Finally, as a simple calibration strategy, we selected a value for the soil moisture threshold parameter that enabled us to best capture observed peak N export (as a function of the NSE). Then using these values, we conducted modeling scenarios to investigate how biogeochemical hotspots influence N export.

Modeling scenarios were based on the presence or absence of biogeochemical hotspots. For the hotspot scenario, we used the optimized soil moisture threshold determined using the approach described above, along with default parameters shown in Table 2, which created "dry" hotspots (i.e., with rapid water diffusion) that had distinct seasonality in denitrification, with very low denitrification during the dry summer, as observed in field data (Li et al., 2006; Parker & Schimel, 2011). In this scenario, the hotspot patches received litter and soil C and N from vegetated patches and both biogeochemical and hydrologic processes still occurred within the hotspot patches. For the non-hotspot scenario, we used unvegetated patches in place of the hotspot patches, in which the soil and vegetation C and N pools were initialized to zero. However, in these unvegetated patches, we did not route litter and passive soil C and N from the vegetated patches. As a result, only hydrologic processes occurred there. We ran these two scenarios for 120 years, 60 years to stabilize the hotspot patches, and another 60 years to compare differences between scenarios.

3 Results

3.1 Initialization and calibration results

Using the target-driven initialization method of Hanan et al. (2018), we were able to capture the spatial distribution of leaf area index (LAI) and associated C stores across the Bell 4 watershed, with some minor underestimates in riparian areas (covered by live oak) and overestimates in a small percentage of patches, which occurred because RHESSys allocates C to LAI at the end of each growing season. Therefore, when the simulated LAI reached its target value in the middle of a growing season, continued growth prior to updating the model stores led to minor overestimation. Overall, the initialized and remotely sensed LAI were a strong match (Figure S1).

During the calibration period, the monthly NSE (a metric to evaluate the extent to which models capture peak streamflow; values close to 1 represent the best correspondence between modeled and observed values) was 0.88. Percent error (a metric to evaluate total flow; values close to 0 represent low error in the total amount of streamflow for modeled vs. observed data) was 5.45%. For the evaluation period, the monthly NSE was 0.8 with a percent error of -3.92%. In general, the model captured the seasonality, recession, and low flow patterns observed in the streamflow record.

3.2 Sensitivity of N fluxes to the abundance of hotspots

As expected, increasing the abundance of hotspots in the model increased N fluxes. The magnitude of increases was generally greatest for nitrification and denitrification, but streamflow N also increased. N flux estimates were sensitive to climate trajectories and key parameters including hotspot abundance, parameters that control hotspot soil moisture, and hotspot connectivity to the surrounding patches. We discuss these in more detail below.

Increasing the abundance of hotspots increased the rate of N fluxes (Figure 6). Specifically, during wet years, the median nitrification rate was 2.48 g N m^{-2} $year^{-1}$ in the non-hotspot scenario while it increased to 4.25 g m^{-2} $year^{-1}$ with 13.7% hotspot cover, representing a 70% increase (Figure 6a). The denitrification rate increased from 0.001 g m^{-2} $year^{-1}$ in the no-hotspot scenario to 0.057 g m^{-2} $year^{-1}$ with 13.7 % hotspot cover, showing a 57-fold increase (Figure 6b). Streamflow nitrate export increased by 76% from 0.816 g m^{-2} $year^{-1}$ to 1.44 g m^{-2} $year^{-1}$ (Figure 6c). When considering cumulative N fluxes over a 60-year period, nitrification increased by 73%, there was a 16-fold increase in denitrification and streamflow nitrate increased by 32% under the 13.7% cover scenario. Thus, the abundance of hotspots had a substantial effect on N processes, particularly denitrification.

Total N export increased with increasing hotspot cover and then reached an asymptote when hotspot cover was greater than 9.1% (Figure 6 b&c). Denitrification rates were very low in the zero percent hotspot cover scenario and increased with an increasing percentage of hotspot patches. However, the rate of increase declined when hotspot cover was greater than 9.1%. Median streamflow nitrate export began increasing when hotspot cover was above 4.5% but reached an asymptote at 9.1%. Maximum streamflow nitrate export also increased with increasing hotspot cover, but the rate of increase declined when cover was above 9.1%. The variability, represented as interquartile ranges, in denitrification and streamflow nitrate both increased and reached an asymptote with increasing percent cover of hotspots (Table S1). This occurred because the total number of patches was the same across different abundance scenarios. Therefore, an increase in hotspot cover corresponded to a concomitant decrease in vegetation cover, which reduced carbon and nitrogen inputs from vegetation to soil. As a result, N cycling processes became limited by plant productivity in a patch family. Although this result was partly an artifact of the model's structure—which resulted in more than one aspatial hotspot patch occurring in some patch families when the hotspot percentage cover exceeded 9.1%—it still demonstrates the mechanism by which increases in hotspot cover above a given threshold can decrease plant productivity. However, the actual threshold value should be interpreted with caution.

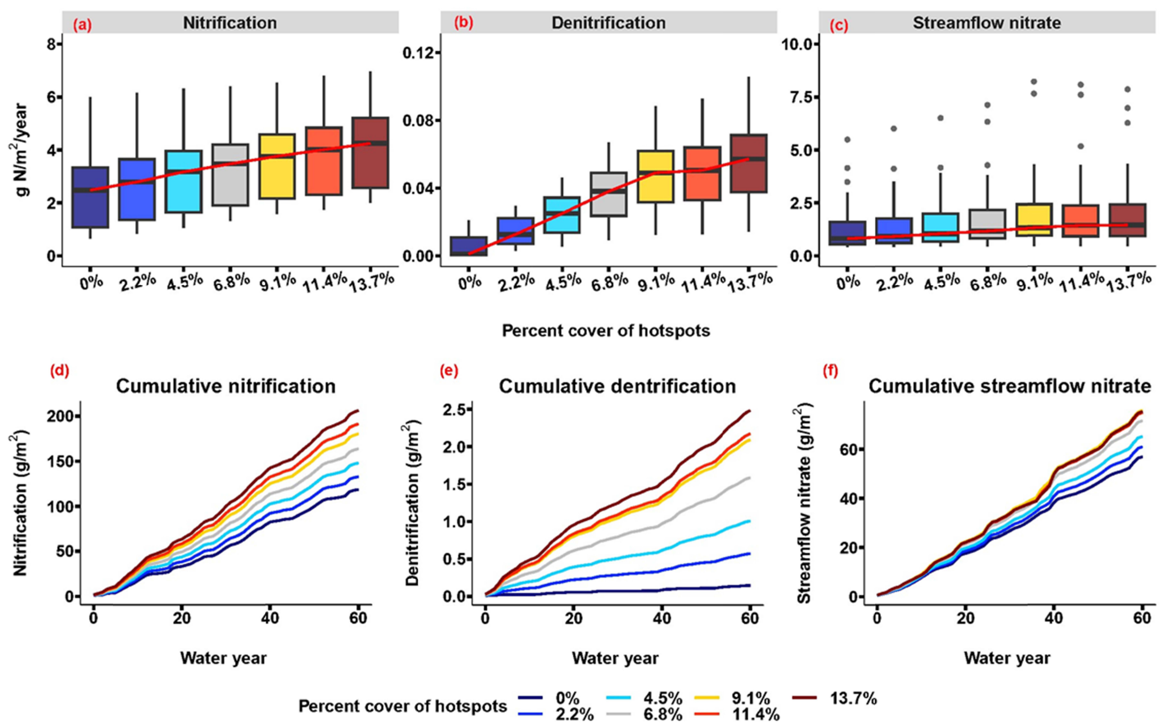

Figure 6. Sensitivity of N processes to the percent cover of hotspots. Panels a, b, and c show the 25^{th}, median, and 75^{th} percentile values and the red line connects the median of each scenario to show the trend. The box plots only consider N fluxes in wet years (when most export occurs; precipitation > 710 mm/year). Panels d, e, and f show cumulative N fluxes over 60 years (including both dry and wet years), different colors represent scenarios with different hotspot percent cover.

3.3 The sensitivity of N fluxes to the parameters controlling water diffusion during periods of hydrologic disconnection.

To examine how the rate at which hotspots dry out during periods of hydrologic disconnection influences N fluxes, we ran three scenarios: a scenario where soil moisture in the hotspots diffused slowly to non-hotspot patches and hotspots retained their soil moisture throughout the year (i.e., a wet hotspot scenario), and a scenario where the diffusion speed was intermediate (i.e., an intermediately-moist hotspot scenario), and a scenario where soil moisture diffused relative quickly from hotspot to non-hotspot patches (i.e., a dry hotspot scenario).

We found that basin-scale nitrification rates can decrease with the moisture content of hotspots (Figure 7 b&g). Higher moisture content in hotspots led to relatively lower moisture content in non-hotspot patches (based on water balance). In the wet-hotspot scenario, basin-scale nitrification was lower than in the dry-hotspot scenario where water slowly diffused to non-hotspot patches. This occurred because in the wet-hotspot scenario, soil moisture in non-hotspot patches was lower, which reduced total nitrification, even though nitrification rates increased in the hotspots. Basin-scale denitrification increased with higher moisture content in hotspots since denitrification mainly occurs in those locations (Figure 7 d&g). For denitrification, the differences between the three scenarios were most pronounced during dry years when soil moisture differences between hotspots and non-hotspot patches were higher (Figure 7 b&d).

During dry and average years, streamflow nitrate export was higher in the scenarios where hotspots remained saturated or close to saturated (i.e., the wet- and intermediately-moist-hotspot scenarios) than in the dry-hotspot scenario where water diffused rapidly during dry periods. This led to more soil N accumulation in the dry-hotspot scenario. However, there was a higher total annual streamflow nitrate export during the wet years in the dry-hotspot scenario especially after multiple dry years (Figure 7c, year 40). Altogether, the closer hotspots are to being water-saturated, the more quickly N is exported to streamflow. During multiple dry years, for the dry hotspot (rapid diffusion) scenario, nitrate accumulated in the saturated zone. Once a wet year occurred, that nitrate was flushed out to streams (Figure 7a and Figure S3, year 40). In the wet hotspot (more continuously saturated) hotspot scenario, higher denitrification, and faster leaching of nitrate from hotspots led to less nitrate accumulation in the saturated zone (Figure S3). In summary, the N movement from soil to streams is driven by an interaction between soil moisture and subsurface flow.

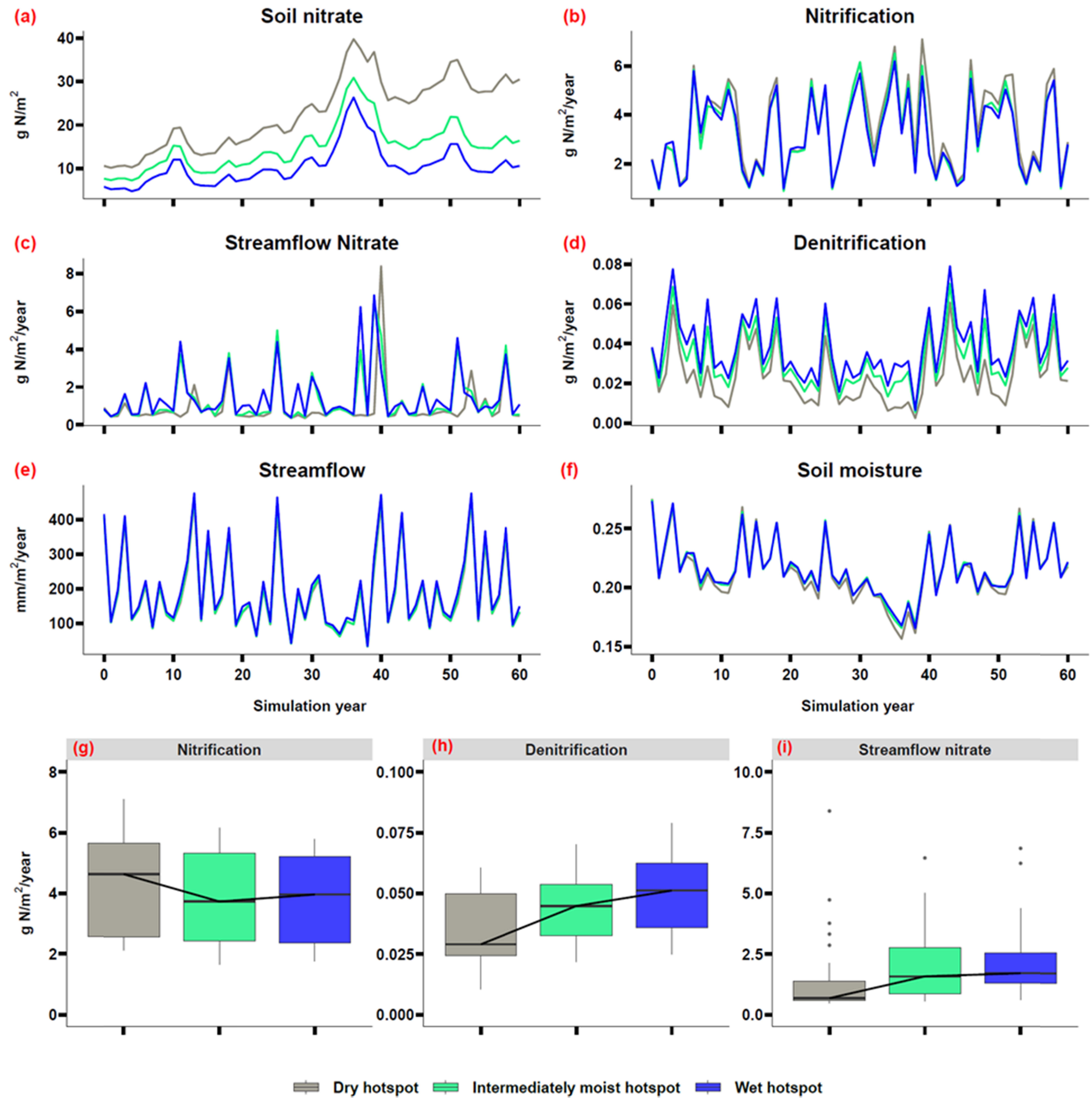

Figure 7. N processes for the three scenarios focused on the rate at which water diffuses from hotspots as soils dry: one where hotspots were saturated most of the time (i.e., the slow diffusion,

wet hotspot scenario), one where water diffused more rapidly from hotspots during the dry season (i.e., the rapid diffusion, dry hotspot scenario), and one where diffusion was intermediate (i.e., the intermediately-moist hotspot scenario). Streamflow is calculated as the average water depth over the basin area of Bell 4 (0.14 km^2). Panels g h and i show the distribution of annual N fluxes in wet years (precipitation > 710 mm/year), box plots show the 25th, median, and 75th percentile values, and the black line connects the median of each scenario.

3.4 Sensitivity of N export to the subsurface connectivity parameter

The soil moisture threshold, which controls the connectivity of hotspots to non-hotspot patches, had a stronger influence on streamflow nitrate export than on nitrification and denitrification fluxes (Figure 8). This occurred because streamflow N export is influenced by both soil moisture content and subsurface lateral transport. Thus, when the threshold was high (i.e., when more moisture was required to establish hydrologic connectivity), streamflow N export was close to zero. With a higher soil moisture threshold, hotspots also tended to have higher moisture content, which increased nitrification and denitrification (Figure 8e), although the increases were small. The soil moisture threshold affected both the magnitude and timing of streamflow nitrate export. At a very low threshold of 0.15, there was a slightly higher amount and similar timing of peak nitrate export to streams compared to the fully connected scenario (i.e., threshold = 0, Figure 8c). These small increases occurred because soil moisture in the non-hotspot patches was higher than 0.15 most of the time (Figure 8d). A threshold of 0.21, which was around the median basin-scale soil moisture, caused the largest peak in streamflow nitrate export. This occurred because connectivity was delayed until the threshold was reached, allowing nitrate to accumulate. When the threshold was larger than 0.21, peak streamflow nitrate was smaller and came later because hotspots were disconnected from non-hotspot patches most of the time.

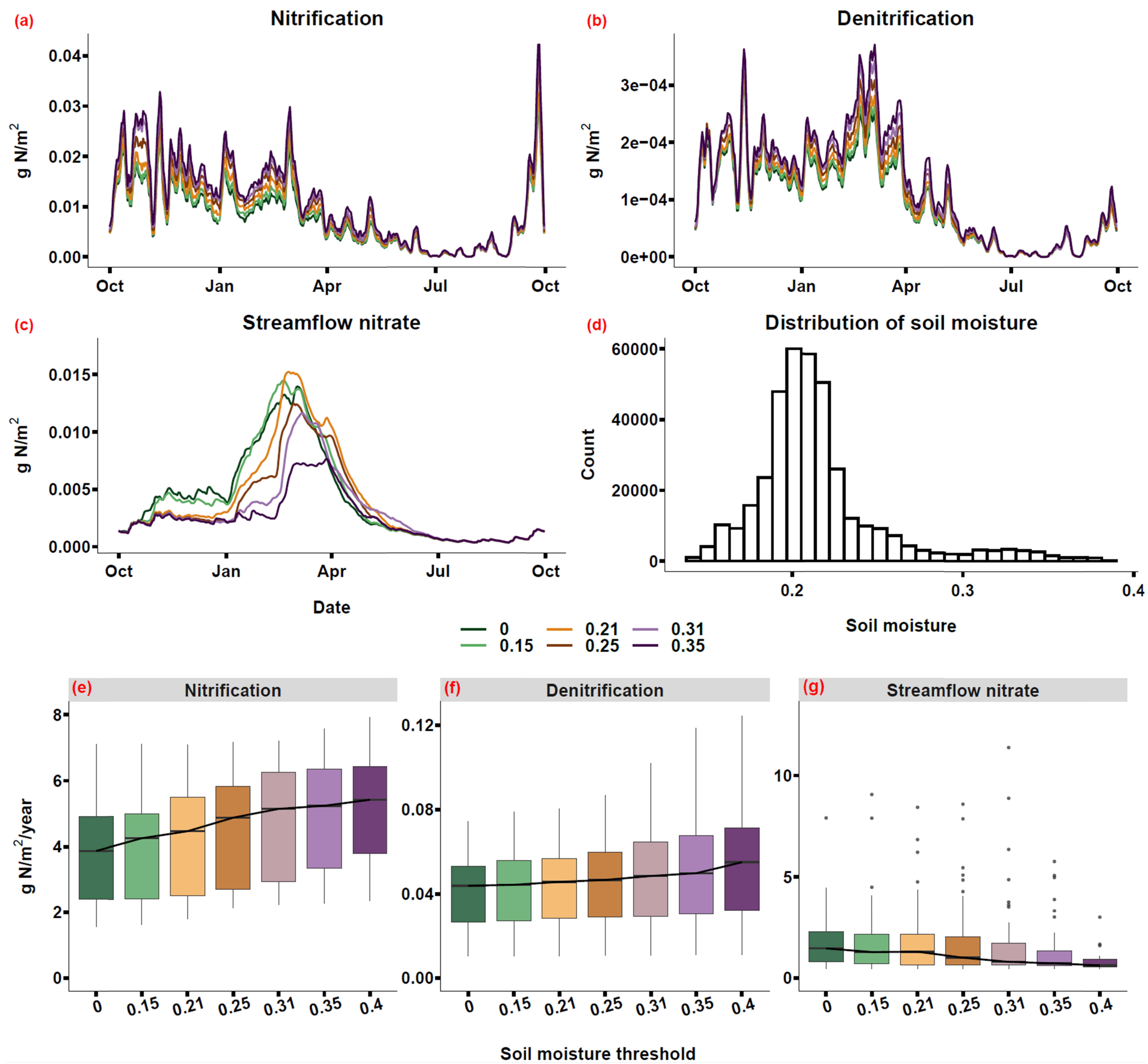

Figure 8. *Sensitivity of N fluxes to the soil moisture threshold. Panels (a), (b) and (c) are mean daily N fluxes over 60 years. Panel (d) is the distribution of daily soil moisture at the basin scale over 60 years. Panels e, f, and g are the distribution of annual fluxes of wet years (precipitation > 700 mm), box plots show 25th, median, 75th percentile, and the black line connects the median of each scenario. Different colors represent different soil moisture thresholds.*

3.5 Prediction of streamflow N export compared with observations.

We selected the best soil moisture threshold from section 3.2 to capture the magnitude of observed nitrate export (i.e., 0.21; this parameter value maximized peak streamflow nitrate export) and we used the default values shown in Table 2 for the other parameters. Using these values, we found that hydrologic disconnection of soil hotspots during the dry periods and reconnection during wet periods enabled us to capture the observed magnitude of nitrate export in streamflow, which we could not otherwise capture in the non-hotspot scenario (Figure 9). For example, the non-hotspot scenario underestimated nitrate export with a NSE of 0.22, while the hotspot scenario increased the estimation peak streamflow nitrate by 29% and captured its timing better with a NSE of 0.4 (in 1988, 1991, 1992, 1993, 2000). However, after selecting the best moisture threshold parameter, the timing of stream nitrate export was still slightly off; for example, in 1998, the modeled stream nitrate export peak was higher and occurred slightly later than observed. Adding a soil moisture threshold to simulate subsurface connectivity may not fully capture the physical processes influencing hotspot moisture dynamics and calibrating sharing coefficients can sometimes lead to equifinality, where multiple parameter sets can yield the similar results. Future research should focus on strategies for reducing parameter uncertainty through strategic observations and developing more mechanistic approaches where needed.

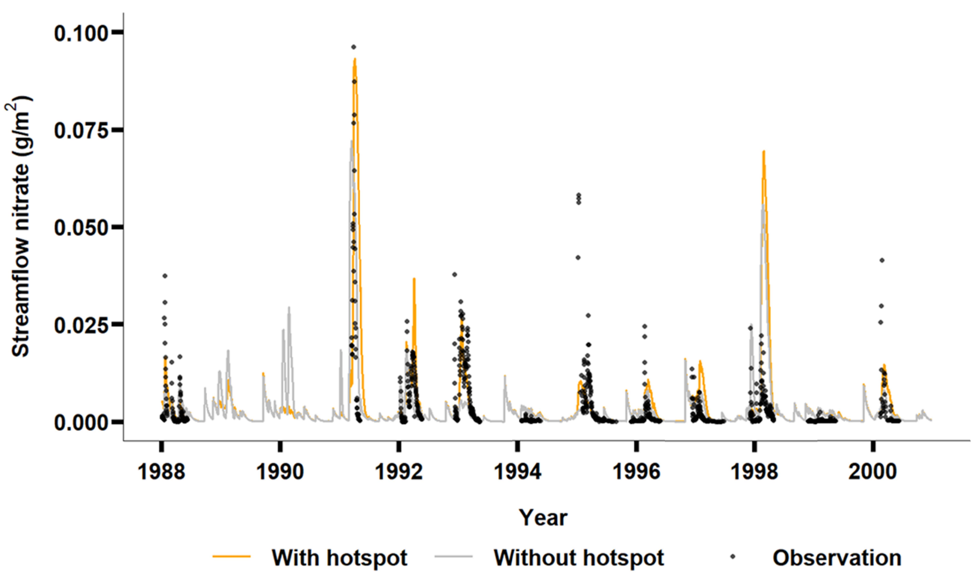

Figure 9. Simulated and observed nitrate export in streamflow.

3.6 Comparison of hotspot and non-hotspot scenarios

At the basin-scale, there was higher N export in the hotspot scenario than in the non-hotspot scenario (Figure 10 a&f). In the hotspot scenario, higher streamflow nitrate export in wet years (e.g., Figure 10c, year 40) corresponded with higher soil nitrate accumulation during the previous dry years (e.g., Figure 10a and Figure S4, year 39). Conversely, less nitrate accumulated during dry years in the non-hotspot scenario (e.g., Figure S4, year 39). Nitrate accumulated during dry years and there was substantial nitrate export to streams in wet years, especially when a wet year followed multiple dry years (e.g., Figure 10c in year 40). We also found that streamflow nitrate export was further influenced by interannual precipitation patterns. The differences between the hotspot and non-hotspot scenarios were most evident during wet years when the basin was more connected (e.g., Figure 10c in years 40 and 53). During wet years, more nitrate was flushed out from hotspots, which illustrates how subsurface connectivity can be an important factor driving streamflow N export. Consequently, the differences in streamflow nitrate between the hotspot and non-hotspot scenarios were less consistent than the differences in nitrification and denitrification, which had similar temporal patterns but differing magnitude (e.g., Figure 10 c&d).

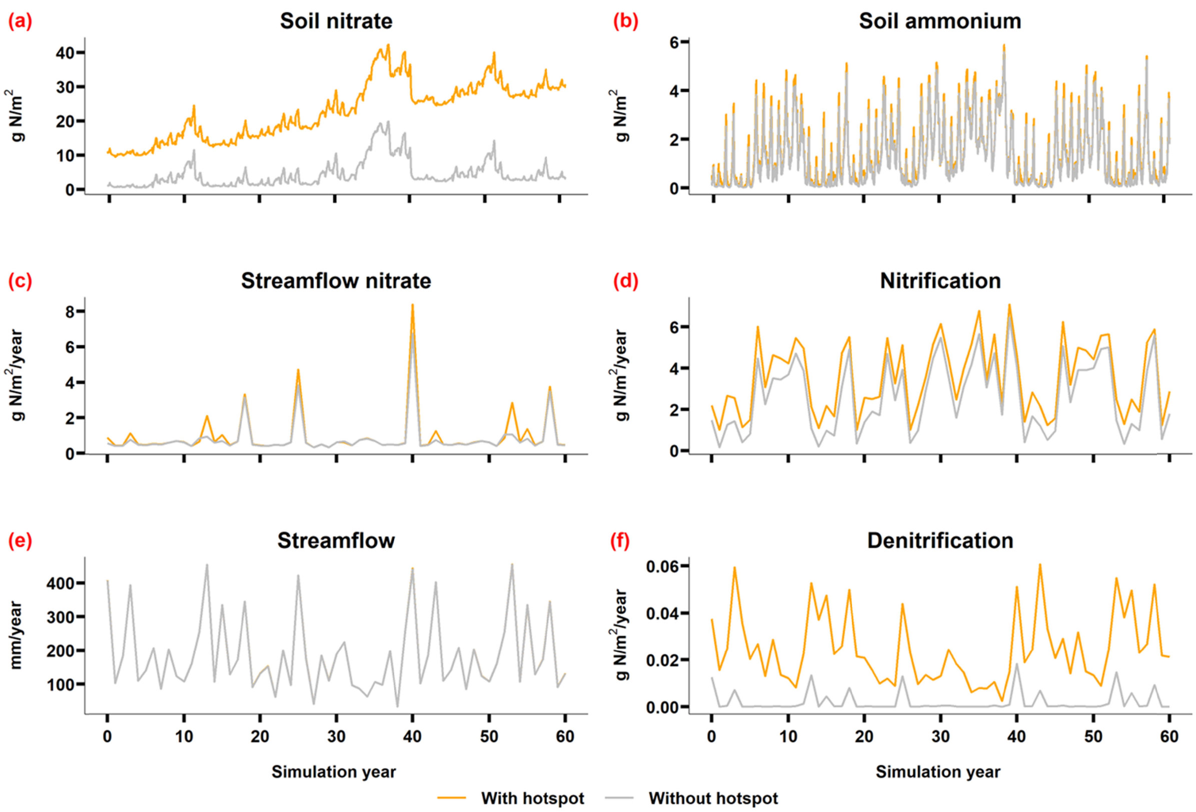

Figure 10. Nitrogen and hydrologic cycling processes (annual sum, streamflow nitrate, nitrification and dentification) and nitrate pools (annual mean, soil nitrate and soil ammonium) for with and without hotspot scenarios at the full basin scale.

4 Discussion

Modeling hotspots at watershed scales has been challenging because most models, including RHESSys, lack corresponding fine-scale (e.g., below 1-meter resolution) parameters and variables (Tague, 2009). To address this limitation, we developed a framework for representing hotspots aspatially within 10-meter resolution patches. Here we define these hotspots as several microscale locations (e.g., soil aggregates) that are distributed aspatially across a 10-meter resolution grid cell. Using this framework, we conducted a series of virtual experiments to investigate how uncertainties in model structure and parameters influence N cycling and export. Then using the new modeling framework, we examined how precipitation can affect N export in a dryland watershed in California. Our model framework and virtual experiments improve our ability to connect field measurements to catchment-scale modeling projections by developing integrative model algorithms and parameters that control the biophysical behavior of hotspots across a landscape. These parameters can be optimized using field observations of N cycling and export. We illustrate how uncertainty in model parameters can influence projections of N export. Future research should aim to reduce these uncertainties, and ultimately represent hotspot behavior more mechanistically across watersheds.

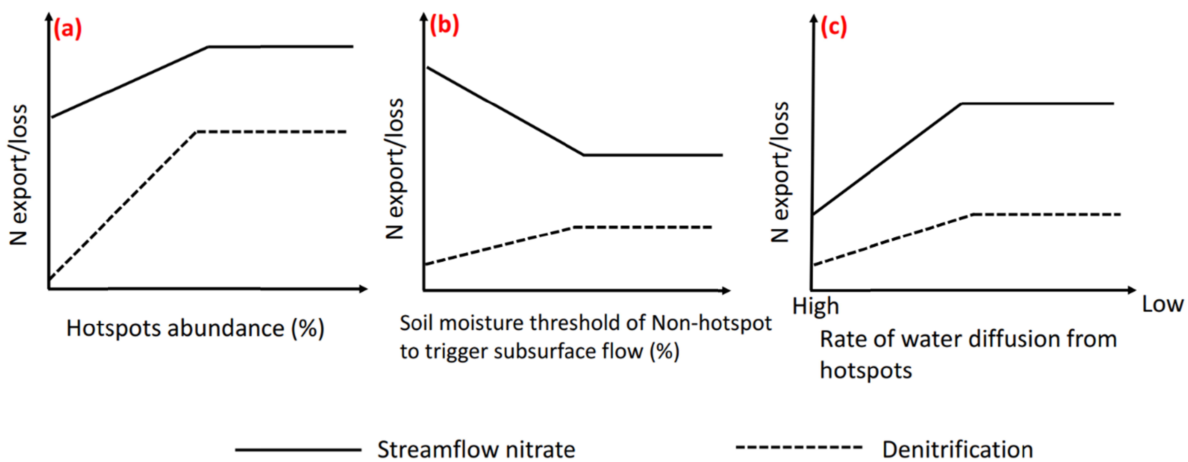

Figure 11. Conceptual framework summarizing how total annual streamflow nitrate and denitrification respond to (a) hotspots abundance, (b) the soil moisture threshold required to trigger subsurface flow, and (c) the rate of water diffusion from hotspots.

4.1. Uncertainties related to hotspot abundance and distribution

Estimating nitrogen (N) export at watershed and regional scales is limited by uncertainty in how hotspots are distributed across landscapes. Our research is among the few studies that have evaluated how hotspot abundance influences watershed-scale N export and illustrates the need to quantify hotspot cover to effectively scale N dynamics from ecosystems to watersheds (Anderson et al., 2015; Groffman, 2012). We parameterized the hotspots with varying percentage cover across a small watershed (0.14 km^2) and found that N export increased with hotspot abundance (Figure 6e and f & Figure 11a), but with an asymptotic relationship due to decreasing N inputs and biogeochemical cycling that occurred when vegetated cover was displaced by hotspot cover. This reduced both nitrification and energy inputs from soil respiration for denitrification (see Eq 9). However, in less N-limited and more mesic sites (e.g., under elevated N deposition and increasing precipitation), N export may be more sensitive to increasing hotspot abundance.

One limitation of our study is that we did not examine how the spatial distribution of hotspots influences N export. Previous research has shown that hotspots can be more concentrated in riparian corridors and wetlands where moisture content is higher (Pinay et al., 2015). We did however find that wet hotspots, which may serve as a surrogate for riparian and wetland locations, can in some cases increase both denitrification and N export in streams (Figure 7 c&d). However, because the location and arrangement of hotspots across a landscape can significantly influence streamflow N export (Laudon et al., 2011; Pinay et al., 2015), more research is needed to understand these spatial relationships (Haas et al., 2013). For example, combing high-resolution remote sensing data with field observations may help us better constrain hotspot distribution and abundance in ecohydrological models (Goodridge et al., 2018; Groffman, 2012; Tague, 2009; Walter et al., 2000).

4.2 Uncertainties in how rapidly hotspots dry out

Soil moisture is a major factor regulating denitrification and streamflow nitrate export (Pinay et al., 2015; Zhu et al., 2012). Our modeling experiments illustrate how the relationships between soil moisture and N dynamics can be complex and non-linear. Elevated soil moisture may reduce nitrification, increase denitrification, and ultimately decrease the amount of nitrate available for hydrologic flushing. Drier soils on the other hand can decrease denitrification and increase the amount of nitrate available for flushing (Homyak et al., 2016). We found that during dry and average years, higher moisture in hotspots increased nitrate infiltration from the unsaturated zone to the saturated zone, resulting in elevated and more rapid nitrate export to streams (Figure 7c). However, during wet years, the wet hotspot scenario had less nitrate export to streams because in prior average years, there was more vertical leaching and therefore less N accumulating in the saturated zone (Figure 7a and Figure S3, year 38-39). The dry hotspot scenario captured the observed nitrate-flushing better than the wet scenario, suggesting that hotspots are not likely to be continuously saturated (Figure 7). Because studies have shown that very small changes in soil moisture can change N fluxes abruptly (Castellano et al., 2013; Evans et al., 2016), it is important to improve our representation of soil moisture conditions in hotspots to accurately predict nitrate export.

Soil water residence time is an important factor affecting N export (Pinay et al., 2015; Zarnetske et al., 2011). The slower water diffuses from hotspots, the longer nitrate is exposed to denitrifying conditions (McClain et al., 2003). Our study shows that when water diffuses more slowly from hotspots (i.e., in the wet hotspot scenario) both denitrification and total N export to streams increase (Figure 7 & Figure 11). We used water diffusion coefficients to modify the rate at which water diffuses from hotspots and we selected coefficients that enabled us to best capture the plausible timing of denitrification and streamflow N fluxes. While this is a simplified, proxy approach, adding further complexity by explicitly modeling diffusion may be infeasible since it would require local, spatially explicit soil parameters (Wood et al., 2011). However, further investigation into how proxy parameters may be calibrated is recommended for future research.

Stream nitrate export was also affected by precipitation patterns. When there were multiple dry years in a row, nitrate accumulated to a greater extent than in average years (Figure

7a). When a wet year followed a multi-year drought, there was higher streamflow nitrate export in the dry hotspot scenario (Figure 7c). This is corroborated by field observations, which suggest that severe drought promoted nitrate accumulation in soil due to less denitrification and plant uptake, resulting in more nitrate available for flushing with the return of precipitation (Winter et al. 2023). We found that the length of drought and precipitation variability were more important in driving streamflow N export than the amount of precipitation (Figure 7c&e). For example, even with similar amount of precipitation in simulation years 26 and 40, N export was much higher in year 40 due to the legacy of a multi-year drought (Figure 7 c&e). Recent research has similarly shown that precipitation variability can have positive or negative legacy effects on dryland productivity, which can in turn influence N cycling and export (Gherardi & Sala, 2015; Krichels et al., 2022). However, the direction of N responses vary along long-term precipitation gradients, such as the response is positive when precipitation is below 300 mm/year and negative when it exceeds 300 mm/year (Gherardi & Sala, 2015, 2019).

4.3 Uncertainties in hydrologic connectivity

The subsurface flow threshold also plays a role in how much nitrate is transported to streams. In this study, we found that the optimal volumetric soil moisture to trigger subsurface flow N export from hotspot to non-hotspot patches was around 21% (Figure 8). Other studies have similarly shown that to trigger a subsurface flow, the soil moisture needs to reach a threshold of 18% (Liao et al., 2016). However, this threshold may vary with soil texture and water potential dynamics. While our new model framework can improve the prediction of streamflow nitrate with a static soil moisture threshold, topography and vegetation cover can also influence the connectivity and amount of subsurface flow, suggesting that soil moisture thresholds should be dynamic (Crow et al., 2012, Zhu et al., 2018).

Coupling soil biogeochemical models with hydrological models has become increasingly popular for investigating N cycling and export (Schimel, 2018). To save time, researchers typically prefer to couple existing models rather than build new ones (Malek et al., 2017; Zhu et al., 2018). Since most hydrologic models do not account for fine-scale heterogeneity in available moisture, they may not be able to capture biogeochemical hotspots even when coupled with biogeochemical models (Chen et al., 2020). Our new model framework provides a relatively simple way to capture hotspots without having to explicitly represent sub-meter scale spatial heterogeneity. While this intermediate complexity approach enables us to represent hotspots across a watershed, it does not fully capture some of the potential controls on hotspot function. For example, although our model captured the variability and magnitude of streamflow nitrate, there was some error associated with its timing (Figure 9). Future work can build upon our simple hotspot model to develop more process-based and dynamic representation of subsurface flow thresholds. This can be achieved by improving our understanding of hydrology and N processes in soil through hydrogeochemical observations.

4.4 The role of hotspots and hot moments in watershed models

We found that the catchment-scale denitrification rate in the hotspot scenarios was significantly higher than that observed in the non-hotspot scenario (Figure 6 & Figure 10), aligning with the concept that small areas often account for a high percentage of denitrification activity (McClain et al., 2003). Additionally, denitrification was more sensitive to hotspot abundance, while N export to streams was more sensitive to the soil moisture threshold that triggers subsurface flow (Figure 11). Still, both are affected by the speed at which water diffuses from hotspots, which influences soil moisture levels, water residence time in soil, and vertical and horizontal transport of water. Our virtual experiments provide information on model uncertainty and sensitivity that can inform future studies focused on scaling N processes from plots to catchments. For example, in areas with high N deposition, managers who are interested in predicting how much N ends up in streams should focus on reducing model uncertainties in subsurface flow thresholds and soil moisture retention in hotspots.

In the context of predicting N export, hot moments—defined as wet periods after a prolonged dry spell (Groffman et al., 2009)—are currently better represented in the RHESSys model than hotspots. Even in our no hotspot scenario, there was a pulse of streamflow N export when wet years followed multiple dry years (Figure 7c & Figure 10c). However, models of how hot moments influence streamflow N export are still limited by uncertainties in soil moisture dynamics. For instance, we found that in the wet hotspot scenario, there was an earlier streamflow N pulse than in the dry hotspot scenario (Figure 7c). Thus, hotspot conditions can affect the timing of hot moments, which has not been previously explored in modeling studies. In future studies, it is important to consider interactions between hotspots and hot moments rather than discussing them in isolation (Bernhardt et al., 2017).

4.5 Implications of future predictions

Our findings highlight the importance of incorporating the role of hotspots when modeling N loss to the atmosphere and N export to streams in dryland ecosystems. Including hotspots substantially increased denitrification, up to 10-fold, and increased streamflow N export by at least 30%. This also improved agreement with stream nitrate data in our study watershed (Figure 6 b&c). Our results also suggest that current biogeochemical models may underestimate N export/loss in drylands when hotspots effect are not considered, particularly following rewetting of dry soils (e.g., Figure 10c, Eberwein et al., 2020; Schimel, 2018).

Denitrification is one of the major sources of greenhouse gas emissions and streamflow N export can affect downstream drinking water quality. For example, the USEPA standard for the maximum contaminant level of nitrate in rivers to protect against blue-baby syndrome is 10 mg L^{-1}, which is equivalent to around 0.5g m^{-2} when the daily peak streamflow is around 50mm m^{-2} day^{-1} (Figure 4a, year 1998; Van Metre et al., 2016). When hotspots were not considered in the model, streamflow N export was underestimated by 0.05g m^{-2} in 1998, representing 10% of the EPA maximum threshold (Figure 9, year 1998). This underestimation could significantly influence longer-term water quality predictions. Future climate change and expanding urbanization will intensify N export/loss by increasing precipitation variability and N deposition (Borer & Stevens, 2022). Therefore, accurate prediction of N export/loss under future environmental change is crucial for mitigating its effects on the environment and society. Our new model framework, which explicitly represents hotspots, proves a valuable tool for water and forest managers to develop strategies aimed at improving water quality and mitigating the effects of environmental change.

5 Conclusion

Coupling hydrologic processes with biogeochemical processes in watershed-scale models is challenging due to subsurface heterogeneity and the existence of hotspots and hot moments that are not well represented in models. We developed a framework for representing hotspots explicitly in dryland watersheds and using this framework, we demonstrated how hydrologic connectivity and precipitation can affect N export in a dryland watershed in California. With increasing hotspot coverage (up to a threshold), both denitrification and N export to streams increased. The partitioning between denitrification and N-export, and the timing and magnitude of N-export were largely controlled by hotspot soil moisture dynamics. Specifically, we found that when the soil moisture threshold required for reestablishing subsurface flow was intermediate, nitrate was able to accumulate during drier periods and then be flushed to the stream upon wet up. This led to the highest peak nitrate export to streams, which tended to better-capture observed nitrate patterns. To our knowledge, this is the first time biogeochemical hotspots have been modeled explicitly using a coupled biogeochemical-ecohydrological model in a dryland watershed. This modeling framework can help better project N export in dryland watersheds where hotspots may play an increasingly important role in governing water quality as drought and N deposition continue to increase.

6 Acknowledgments

This project was supported by National Science Foundation of the United States under award number DEB-1916658. We thank Tom Dilts for helping with preparing input maps and data of RHESSys. We thank Pete Wohlgemuth for helping with streamflow data processing and model calibration. This study was supported in part by the USDA Forest Service Rocky Mountain Research Station. The findings and conclusions in this publication are those of the author and should not be construed to represent any official USDA or U.S. Government determination or policy.

Conflict of Interest

The authors declare no conflicts of interest relevant to this study.

Data Availability Statement

The data sets used to run simulations for this study can be found in the Open Science Forum: https://doi.org/10.17605/OSF.IO/UKPJG (Ren et al., 2023a), and the model code can be found on GitHub: https://doi.org/10.5281/zenodo.7754375 (Ren et al., 2023b).

References

Abatzoglou, J. T. (2013). Development of gridded surface meteorological data for ecological applications and modelling. *International Journal of Climatology*, *33*(1), 121–131. https://doi.org/10.1002/joc.3413

Anderson, T. R., Groffman, P. M., & Walter, M. T. (2015). Using a soil topographic index to distribute denitrification fluxes across a northeastern headwater catchment. *Journal of Hydrology*, *522*, 123–134. https://doi.org/10.1016/j.jhydrol.2014.12.043

Baret, F., Olioso, A., Luciani, J. L., Hanocq, J. F., & Monterrot, J. C. (1989). Estimation à partir de mesures de réflectance spectrale du rayonnement photosynthétiquement actif absorbé par une culture de blé. *Agronomie*, *9*(9), 885–895. https://doi.org/10.1051/agro:19890906

Bernhardt, E. S., Blaszczak, J. R., Ficken, C. D., Fork, M. L., Kaiser, K. E., & Seybold, E. C. (2017). Control Points in Ecosystems: Moving Beyond the Hot Spot Hot Moment Concept. *Ecosystems*, *20*(4), 665–682. https://doi.org/10.1007/s10021-016-0103-y

Borer, E. T., & Stevens, C. J. (2022). Nitrogen deposition and climate: an integrated synthesis. *Trends in Ecology & Evolution*. https://doi.org/10.1016/j.tree.2022.02.013

Burke, W. D., Tague, C., Kennedy, M. C., & Moritz, M. A. (2021). Understanding How Fuel Treatments Interact With Climate and Biophysical Setting to Affect Fire, Water, and Forest Health: A Process-Based Modeling Approach. *Frontiers in Forests and Global Change*, *3*. https://doi.org/10.3389/ffgc.2020.591162

Castellano, M. J., Lewis, D. B., & Kaye, J. P. (2013). Response of soil nitrogen retention to the interactive effects of soil texture, hydrology, and organic matter. *Journal of Geophysical Research: Biogeosciences*, *118*(1), 280–290. https://doi.org/10.1002/jgrg.20015

Chaney, N. W., Wood, E. F., McBratney, A. B., Hempel, J. W., Nauman, T. W., Brungard, C. W., & Odgers, N. P. (2016). POLARIS: A 30-meter probabilistic soil series map of the contiguous United States. *Geoderma*, *274*, 54–67. https://doi.org/10.1016/j.geoderma.2016.03.025

Chen, X., Tague, C. L., Melack, J. M., & Keller, A. A. (2020). Sensitivity of nitrate concentration-discharge patterns to soil nitrate distribution and drainage properties in the vertical dimension. *Hydrological Processes*, *34*(11), 2477–2493. https://doi.org/10.1002/hyp.13742

Clark, M. P., Bierkens, M. F. P., Samaniego, L., Woods, R. A., Uijlenhoet, R., Bennett, K. E., et al. (2017). The evolution of process-based hydrologic models: historical challenges and the collective quest for physical realism. *Hydrology and Earth System Sciences*, *21*(7), 3427–3440. https://doi.org/10.5194/hess-21-3427-2017

Crow, W. T., Berg, A. A., Cosh, M. H., Loew, A., Mohanty, B. P., Panciera, R., et al. (2012). Upscaling sparse ground-based soil moisture observations for the validation of coarse-resolution satellite soil moisture products. *Reviews of Geophysics*, *50*(2). https://doi.org/10.1029/2011RG000372

Dunn, P. H., Barro, S. C., Wells, W. G., Poth, M. A., Wohlgemuth, P. M., & Colver, C. G. (1988). *The San Dimas experimental forest: 50 years of research* (No. PSW-GTR-104) (p. PSW-GTR-104). Berkeley, CA: U.S. Department of Agriculture, Forest Service, Pacific Southwest Forest and Range Experiment Station. https://doi.org/10.2737/PSW-GTR-104

Eagleson, P. S. (1978). Climate, soil, and vegetation: 3. A simplified model of soil moisture movement in the liquid phase. *Water Resources Research*, *14*(5), 722–730. https://doi.org/10.1029/WR014i005p00722

Eberwein, J. R., Homyak, P. M., Carey, C. J., Aronson, E. L., & Jenerette, G. D. (2020). Large nitrogen oxide emission pulses from desert soils and associated microbiomes. *Biogeochemistry*, *149*(3), 239–250. https://doi.org/10.1007/s10533-020-00672-9

Ebrahimi, A., & Or, D. (2018). On Upscaling of Soil Microbial Processes and Biogeochemical Fluxes From Aggregates to Landscapes. *Journal of Geophysical Research: Biogeosciences*, *123*(5), 1526–1547. https://doi.org/10.1029/2017JG004347

Evans, S., Dieckmann, U., Franklin, O., & Kaiser, C. (2016). Synergistic effects of diffusion and microbial physiology reproduce the Birch effect in a micro-scale model. *Soil Biology and Biochemistry*, *93*, 28–37. https://doi.org/10.1016/j.soilbio.2015.10.020

Fenn, M. E., Baron, J. S., Allen, E. B., Rueth, H. M., Nydick, K. R., Geiser, L., et al. (2003). Ecological Effects of Nitrogen Deposition in the Western United States. *BioScience*, *53*(4), 404–420. https://doi.org/10.1641/0006-3568(2003)053[0404:EEONDI]2.0.CO;2

Garcia, E. S., Tague, C. L., & Choate, J. S. (2016). Uncertainty in carbon allocation strategy and ecophysiological parameterization influences on carbon and streamflow estimates for two western US forested watersheds. *Ecological Modelling*, *342*, 19–33. https://doi.org/10.1016/j.ecolmodel.2016.09.021

Garson, D. C., & Lacaze, B. (2003). Monitoring Leaf Area Index of Mediterranean oak woodlands: Comparison of remotely-sensed estimates with simulations from an ecological process-based model. *International Journal of Remote Sensing*, *24*(17), 3441–3456. https://doi.org/10.1080/0143116021000024267

Gherardi, L. A., & Sala, O. E. (2015). Enhanced precipitation variability decreases grass- and increases shrub-productivity. *Proceedings of the National Academy of Sciences*, *112*(41), 12735–12740. https://doi.org/10.1073/pnas.1506433112

Gherardi, L. A., & Sala, O. E. (2019). Effect of interannual precipitation variability on dryland productivity: A global synthesis. *Global Change Biology*, *25*(1), 269–276. https://doi.org/10.1111/gcb.14480

Goodridge, B. M., Hanan, E. J., Aguilera, R., Wetherley, E. B., Chen, Y.-J., D'Antonio, C. M., & Melack, J. M. (2018). Retention of Nitrogen Following Wildfire in a Chaparral Ecosystem. *Ecosystems*, *21*(8), 1608–1622. https://doi.org/10.1007/s10021-018-0243-3

Groffman, P. M. (2012). Terrestrial denitrification: challenges and opportunities. *Ecological Processes*, *1*(1), 1–11. https://doi.org/10.1186/2192-1709-1-11

Groffman, P. M., Butterbach-Bahl, K., Fulweiler, R. W., Gold, A. J., Morse, J. L., Stander, E. K., et al. (2009). Challenges to incorporating spatially and temporally explicit phenomena (hotspots and hot moments) in denitrification models. *Biogeochemistry*, *93*(1–2), 49–77. https://doi.org/10.1007/s10533-008-9277-5

Gustine, R. N., Hanan, E. J., Robichaud, P. R., & Elliot, W. J. (2022). From burned slopes to streams: how wildfire affects nitrogen cycling and retention in forests and fire-prone watersheds. *Biogeochemistry*, *157*(1), 51–68. https://doi.org/10.1007/s10533-021-00861-0

Haas, E., Klatt, S., Fröhlich, A., Kraft, P., Werner, C., Kiese, R., et al. (2013). LandscapeDNDC: a process model for simulation of biosphere–atmosphere–hydrosphere exchange processes at site and regional scale. *Landscape Ecology*, *28*(4), 615–636. https://doi.org/10.1007/s10980-012-9772-x

Hallaq, A. (2010). The impact of soil texture on nitrates leaching into groundwater in the north governorate, Gaza strip. *Journal of the Social Sciences*, *38*, 11–35.

Hanan, E. J., Tague, C. (Naomi), & Schimel, J. P. (2017). Nitrogen cycling and export in California chaparral: the role of climate in shaping ecosystem responses to fire. *Ecological Monographs*, *87*(1), 76–90. https://doi.org/10.1002/ecm.1234

Hanan, E. J., Tague, C., Choate, J., Liu, M., Kolden, C., & Adam, J. (2018). Accounting for disturbance history in models: using remote sensing to constrain carbon and nitrogen pool spin-up. *Ecological Applications: A Publication of the Ecological Society of America*, *28*(5), 1197–1214. https://doi.org/10.1002/eap.1718

Hanan, E. J., Ren, J., Tague, C. L., Kolden, C. A., Abatzoglou, J. T., Bart, R. R., et al. (2021). How climate change and fire exclusion drive wildfire regimes at actionable scales. *Environmental Research Letters*, *16*(2), 024051. https://doi.org/10.1088/1748-9326/abd78e

Hartigan, J. A., & Wong, M. A. (1979). Algorithm AS 136: A K-Means Clustering Algorithm. *Journal of the Royal Statistical Society. Series C (Applied Statistics)*, *28*(1), 100–108. https://doi.org/10.2307/2346830

Hassink, J. (1994). Effects of soil texture and grassland management on soil organic C and N and rates of C and N mineralization. *Soil Biology and Biochemistry*, *26*(9), 1221–1231. https://doi.org/10.1016/0038-0717(94)90147-3

Homyak, P. M., Sickman, J. O., Miller, A. E., Melack, J. M., Meixner, T., & Schimel, J. P. (2014). Assessing Nitrogen-Saturation in a Seasonally Dry Chaparral Watershed: Limitations of Traditional Indicators of N-Saturation. *Ecosystems*, *17*(7), 1286–1305. https://doi.org/10.1007/s10021-014-9792-2

Homyak, P. M., Blankinship, J. C., Marchus, K., Lucero, D. M., Sickman, J. O., & Schimel, J. P. (2016). Aridity and plant uptake interact to make dryland soils hotspots for nitric oxide (NO) emissions. *Proceedings of the National Academy of Sciences*, *113*(19), E2608–E2616. https://doi.org/10.1073/pnas.1520496113

Krichels, A. H., Greene, A. C., Jenerette, G. D., Spasojevic, M. J., Glassman, S. I., & Homyak, P. M. (2022). Precipitation legacies amplify ecosystem nitrogen losses from nitric oxide emissions in a Pinyon–Juniper dryland. *Ecology*, *104*(2), e3930. https://doi.org/10.1002/ecy.3930

Laudon, H., Berggren, M., Ågren, A., Buffam, I., Bishop, K., Grabs, T., et al. (2011). Patterns and Dynamics of Dissolved Organic Carbon (DOC) in Boreal Streams: The Role of Processes, Connectivity, and Scaling. *Ecosystems*, *14*(6), 880–893. https://doi.org/10.1007/s10021-011-9452-8

Li, X., Meixner, T., Sickman, J. O., Miller, A. E., Schimel, J. P., & Melack, J. M. (2006). Decadal-scale Dynamics of Water, Carbon and Nitrogen in a California Chaparral Ecosystem: DAYCENT Modeling Results. *Biogeochemistry*, *77*(2), 217–245. https://doi.org/10.1007/s10533-005-1391-z

Liao, K.-H., Lv, L.-G., Yang, G.-S., & Zhu, Q. (2016). Sensitivity of simulated hillslope subsurface flow to rainfall patterns, soil texture and land use. *Soil Use and Management*, *32*(3), 422–432. https://doi.org/10.1111/sum.12282

Lin, L., Webster, J. R., Hwang, T., & Band, L. E. (2015). Effects of lateral nitrate flux and instream processes on dissolved inorganic nitrogen export in a forested catchment: A model sensitivity analysis. *Water Resources Research*, *51*(4), 2680–2695. https://doi.org/10.1002/2014WR015962

Malek, K., Stöckle, C., Chinnayakanahalli, K., Nelson, R., Liu, M., Rajagopalan, K., et al. (2017). VIC–CropSyst-v2: A regional-scale modeling platform to simulate the nexus of climate, hydrology, cropping systems, and human decisions. *Geoscientific Model Development*, *10*(8), 3059–3084. https://doi.org/10.5194/gmd-10-3059-2017

Maxwell, A. E., Warner, T. A., Vanderbilt, B. C., & Ramezan, C. A. (2017). Land Cover Classification and Feature Extraction from National Agriculture Imagery Program (NAIP) Orthoimagery: A Review. *Photogrammetric Engineering & Remote Sensing*, *83*(11), 737–747. https://doi.org/10.14358/PERS.83.10.737

McClain, M. E., Boyer, E. W., Dent, C. L., Gergel, S. E., Grimm, N. B., Groffman, P. M., et al. (2003). Biogeochemical Hot Spots and Hot Moments at the Interface of Terrestrial and Aquatic Ecosystems. *Ecosystems*, *6*(4), 301–312. https://doi.org/10.1007/s10021-003-0161-9

McMichael, C. E., Hope, A. S., Roberts, D. A., & Anaya, M. R. (2004). Post-fire recovery of leaf area index in California chaparral: A remote sensing-chronosequence approach. *International Journal of Remote Sensing*, *25*(21), 4743–4760. https://doi.org/10.1080/01431160410001726067

Meentemeyer, R. K., & Moody, A. (2002). Distribution of plant life history types in California chaparral: the role of topographically-determined drought severity. *Journal of Vegetation Science*, *13*(1), 67–78. https://doi.org/10.1111/j.1654-1103.2002.tb02024.x

Meixner, T., Fenn, M. E., Wohlgemuth, P., Oxford, M., & Riggan, P. (2006). N Saturation Symptoms in Chaparral Catchments Are Not Reversed by Prescribed Fire. *Environmental Science & Technology*, *40*(9), 2887–2894. https://doi.org/10.1021/es051268z

Nash, J. E., & Sutcliffe, J. V. (1970). River flow forecasting through conceptual models part I — A discussion of principles. *Journal of Hydrology*, *10*(3), 282–290. https://doi.org/10.1016/0022-1694(70)90255-6

Osborne, B. B., Nasto, M. K., Soper, F. M., Asner, G. P., Balzotti, C. S., Cleveland, C. C., et al. (2020). Leaf litter inputs reinforce islands of nitrogen fertility in a lowland tropical forest. *Biogeochemistry*, *147*(3), 293–306. https://doi.org/10.1007/s10533-020-00643-0

Ouyang, W., Xu, X., Hao, Z., & Gao, X. (2017). Effects of soil moisture content on upland nitrogen loss. *Journal of Hydrology*, *546*, 71–80. https://doi.org/10.1016/j.jhydrol.2016.12.053

Parker, S. S., & Schimel, J. P. (2011). Soil nitrogen availability and transformations differ between the summer and the growing season in a California grassland. *Applied Soil Ecology*, *48*(2), 185–192. https://doi.org/10.1016/j.apsoil.2011.03.007

Parton, W. J. (1996). The CENTURY model. In D. S. Powlson, P. Smith, & J. U. Smith (Eds.), *Evaluation of Soil Organic Matter Models* (Vol. 38, pp. 283–291). Springer, Berlin, Heidelberg: Evaluation of Soil Organic Matter Models.

Phillip, J. (1957). The theory of infiltration: 4. Sorptivity and algebraic infiltration equation. *Soil Sci*, *84*, 257–264.

Pinay, G., Peiffer, S., De Dreuzy, J.-R., Krause, S., Hannah, D. M., Fleckenstein, J. H., et al. (2015). Upscaling Nitrogen Removal Capacity from Local Hotspots to Low Stream Orders' Drainage Basins. *Ecosystems*, *18*(6), 1101–1120. https://doi.org/10.1007/s10021-015-9878-5

Poblador, S., Lupon, A., Sabaté, S., & Sabater, F. (2017). Soil water content drives spatiotemporal patterns of CO_2 and N_2O emissions from a Mediterranean riparian forest soil. *Biogeosciences*, *14*(18), 4195–4208. https://doi.org/10.5194/bg-14-4195-2017

R Core Team. (2022). R: A Language and Environment for Statistical Computing. Retrieved from https://www.R-project.org/

Ren, J., Adam, J. C., Hicke, J. A., Hanan, E. J., Tague, C. L., Liu, M., et al. (2021). How does water yield respond to mountain pine beetle infestation in a semiarid forest? *Hydrology and Earth System Sciences*, *25*(9), 4681–4699. https://doi.org/10.5194/hess-25-4681-2021

Ren, J., Hanan, E. J., Abatzoglou, J. T., Kolden, C. A., Tague, C. (Naomi) L., Kennedy, M. C., et al. (2022). Projecting Future Fire Regimes in a Semiarid Watershed of the Inland Northwestern United States: Interactions Among Climate Change, Vegetation Productivity, and Fuel Dynamics. *Earth's Future*, *10*(3), e2021EF002518. https://doi.org/10.1029/2021EF002518

Ren, J., Hanan, E. J., Greene A., Tague, C. L., Krichels, A. H., Burke, W. D., Schimel, J. P., Homyak, P. M. (2023a) Code for simulating the role of biogeochemical hotspots in driving nitrogen export from drylands watersheds (Version 7.4) [Software]. Zenodo. https://doi.org/10.5281/zenodo.7754375

Ren, J., Hanan, E. J., Greene A., Tague, C. L., Krichels, A. H., Burke, W. D., Schimel, J. P., Homyak, P. M. (2023b) Data for simulating the role of biogeochemical hotspots in driving nitrogen export from drylands watersheds (Version 7.4) [Dataset]. Open Science Forum. https://doi.org/10.17605/OSF.IO/UKPJG

Ridolfi, L., Laio, F., & D’Odorico, P. (2008). Fertility Island Formation and Evolution in Dryland Ecosystems. *Ecology and Society*, *13*(1). https://doi.org/10.5751/ES-02302-130105

Schimel, J. P. (2018). Life in Dry Soils: Effects of Drought on Soil Microbial Communities and Processes. *Annual Review of Ecology, Evolution, and Systematics*, *49*(1), 409–432. https://doi.org/10.1146/annurev-ecolsys-110617-062614

Schmidt, J. P., Hong, N., Dellinger, A., Beegle, D. B., & Lin, H. (2007). Hillslope Variability in Corn Response to Nitrogen Linked to In-Season Soil Moisture Redistribution. *Agronomy Journal*, *99*(1), 229–237. https://doi.org/10.2134/agronj2006.0187

Seager, R., Lis, N., Feldman, J., Ting, M., Williams, A. P., Nakamura, J., et al. (2018). Whither the 100th Meridian? The Once and Future Physical and Human Geography of America’s Arid–Humid Divide. Part I: The Story So Far. *Earth Interactions*, *22*(5), 1–22. https://doi.org/10.1175/EI-D-17-0011.1

Smith, F. W., Sampson, D. A., & Long, J. N. (1991). Comparison of Leaf Area Index Estimates from Tree Allometrics and Measured Light Interception. *Forest Science*, *37*(6), 1682–1688. https://doi.org/10.1093/forestscience/37.6.1682

Soil Survey Staff. (2022). *Keys to Soil Taxonomy, 13th ed.* USDA-Natural Resources.

Tague, C. (2009). Modeling hydrologic controls on denitrification: sensitivity to parameter uncertainty and landscape representation. *Biogeochemistry*, *93*(1/2,), 79–90.

Tague, C. L., & Band, L. E. (2004). RHESSys: Regional Hydro-Ecologic Simulation System—An Object-Oriented Approach to Spatially Distributed Modeling of Carbon, Water, and Nutrient Cycling. *Earth Interactions*, *8*(19), 1–42. https://doi.org/10.1175/1087-3562(2004)8<1:RRHSSO>2.0.CO;2

Van Metre, P. C., Frey, J. W., Musgrove, M., Nakagaki, N., Qi, S., Mahler, B. J., et al. (2016). High Nitrate Concentrations in Some Midwest United States Streams in 2013 after the 2012 Drought. *Journal of Environmental Quality*, *45*(5), 1696–1704. https://doi.org/10.2134/jeq2015.12.0591

Walter, M. T., Walter, M. F., Brooks, E. S., Steenhuis, T. S., Boll, J., & Weiler, K. (2000). Hydrologically sensitive areas: Variable source area hydrology implications for water quality risk assessment. *Journal of Soil and Water Conservation*, *55*(3), 277–284.

White, M. A., Thornton, P. E., Running, S. W., & Nemani, R. R. (2000). Parameterization and Sensitivity Analysis of the BIOME–BGC Terrestrial Ecosystem Model: Net Primary Production Controls. *Earth Interactions*, *4*(3), 1–85. https://doi.org/10.1175/1087-3562(2000)004<0003:PASAOT>2.0.CO;2

Witheetrirong, Y., Tripathi, N. K., Tipdecho, T., & Parkpian, P. (2011). Estimation of the Effect of Soil Texture on Nitrate-Nitrogen Content in Groundwater Using Optical Remote Sensing. *International Journal of Environmental Research and Public Health*, *8*(8), 3416–3436. https://doi.org/10.3390/ijerph8083416

Wohlgemuth, P. (2006). *Hillslope erosion and small watershed sediment yield following a wildfire on the San Dimas Experimental Forest, southern California*. Reno, Nevada.: Proceedings of the 8th Federal Interagency Sedimentation Conference. Retrieved from https://www.semanticscholar.org/paper/HILLSLOPE-EROSION-AND-SMALL-WATERSHED-SEDIMENT-A-ON-Wohlgemuth/e666a9991c2c1813f3e63289a20636d4028fb7ec

Wood, E. F., Lettenmaier, D. P., & Zartarian, V. G. (1992). A land-surface hydrology parameterization with subgrid variability for general circulation models. *Journal of*

Geophysical Research: Atmospheres, *97*(D3), 2717–2728. https://doi.org/10.1029/91JD01786

Wood, E. F., Roundy, J. K., Troy, T. J., van Beek, L. P. H., Bierkens, M. F. P., Blyth, E., et al. (2011). Hyperresolution global land surface modeling: Meeting a grand challenge for monitoring Earth's terrestrial water. *Water Resources Research*, *47*(5). https://doi.org/10.1029/2010WR010090

Zarnetske, J. P., Haggerty, R., Wondzell, S. M., & Baker, M. A. (2011). Dynamics of nitrate production and removal as a function of residence time in the hyporheic zone. *Journal of Geophysical Research: Biogeosciences*, *116*(G1). https://doi.org/10.1029/2010JG001356

Zhang, J., Cai, Z., & Müller, C. (2018). Terrestrial N cycling associated with climate and plant-specific N preferences: a review. *European Journal of Soil Science*, *69*(3), 488–501. https://doi.org/10.1111/ejss.12533

Zhu, Q., Schmidt, J. P., & Bryant, R. B. (2012). Hot moments and hot spots of nutrient losses from a mixed land use watershed. *Journal of Hydrology*, *414–415*, 393–404. https://doi.org/10.1016/j.jhydrol.2011.11.011

Zhu, Q., Schmidt, J. P., & Bryant, R. B. (2015). Maize (Zea mays L.) yield response to nitrogen as influenced by spatio-temporal variations of soil–water-topography dynamics. *Soil and Tillage Research*, *146*, 174–183. https://doi.org/10.1016/j.still.2014.10.006

Zhu, Q., Castellano, M. J., & Yang, G. (2018). Coupling soil water processes and the nitrogen cycle across spatial scales: Potentials, bottlenecks and solutions. *Earth-Science Reviews*, *187*, 248–258. https://doi.org/10.1016/j.earscirev.2018.10.005

Figure 1.

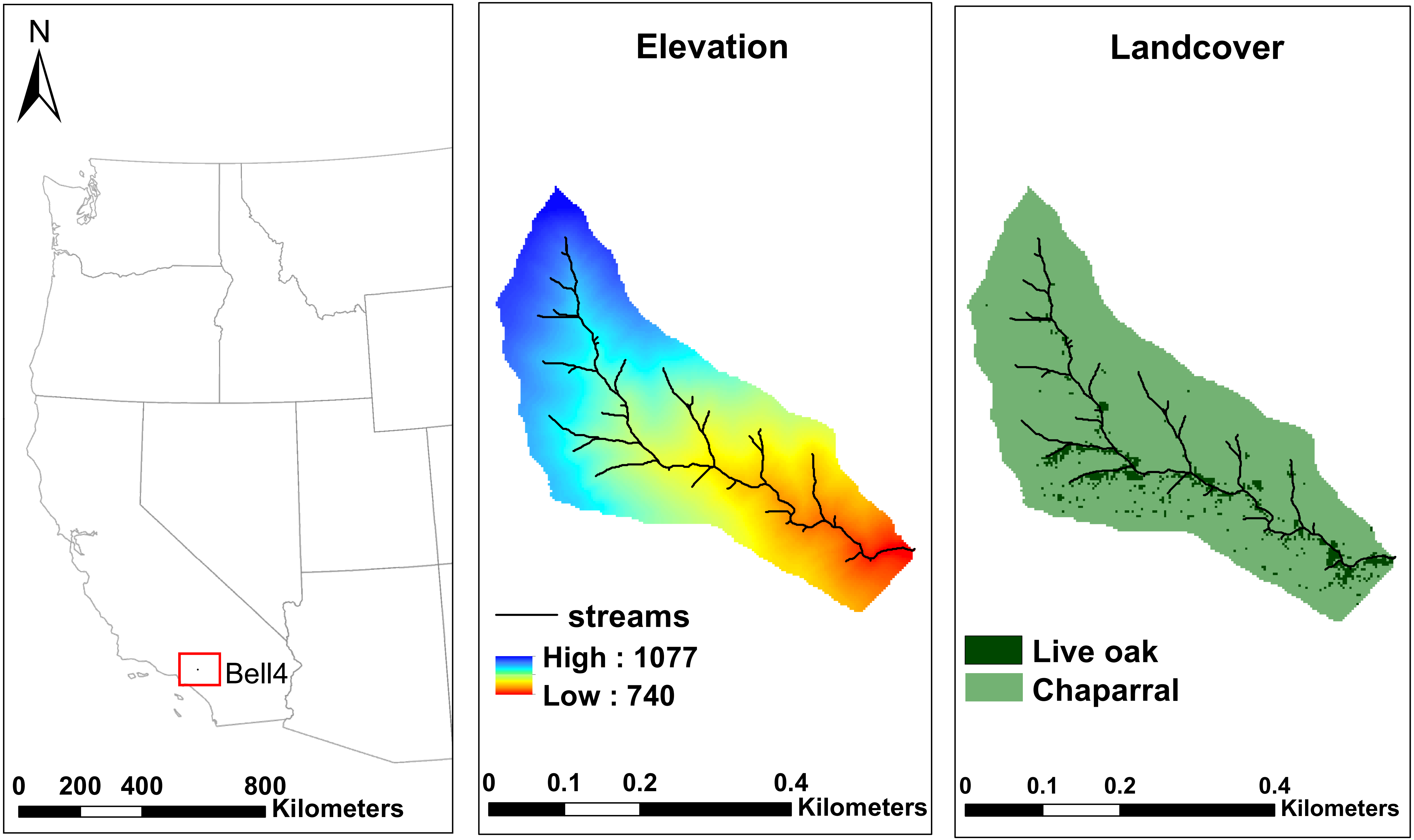

N
Bell4
0 200 400 800
Kilometers
Elevation
streams
High : 1077
Low : 740
0 0.1 0.2 0.4
Kilometers
Landcover
Live oak
Chaparral
0 0.1 0.2 0.4
Kilometers

Figure 2.

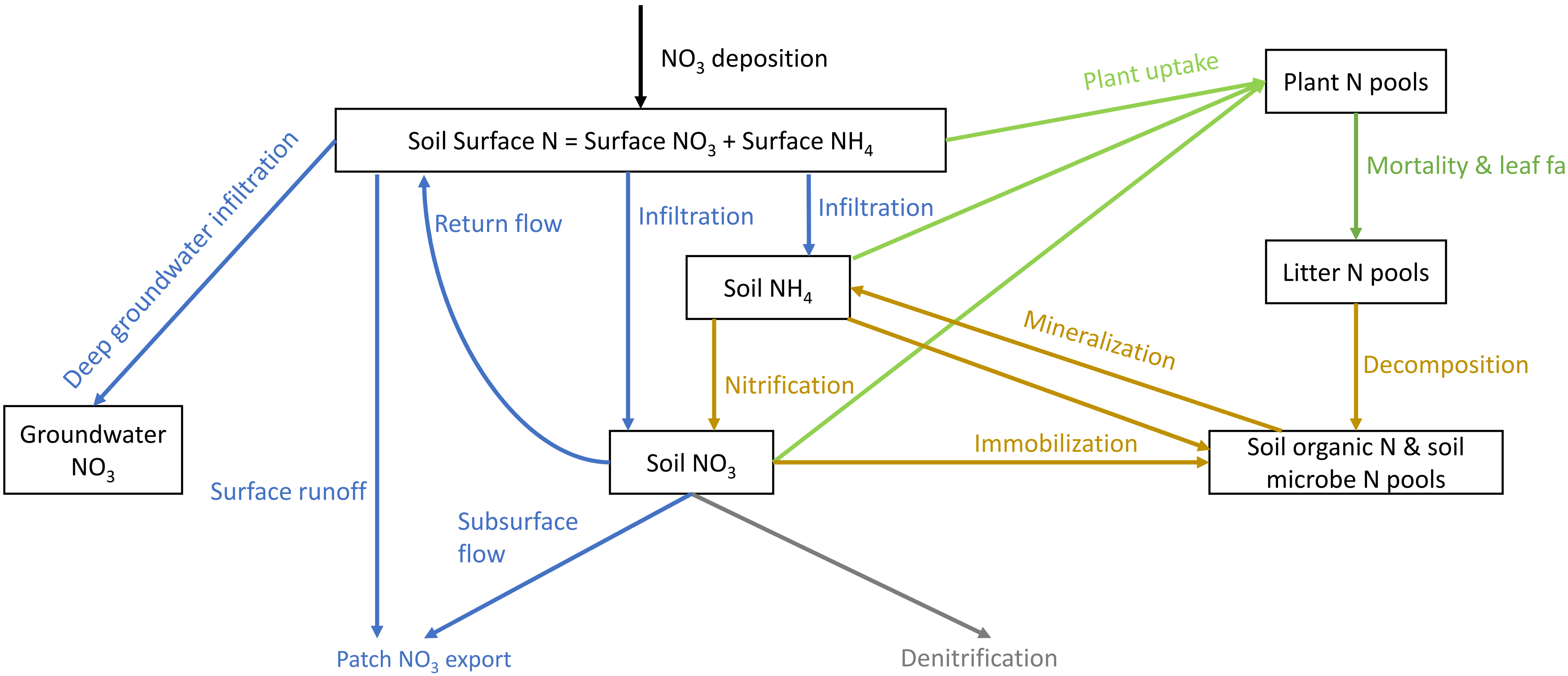

NO_3 deposition
Soil Surface N = Surface NO_3 + Surface NH_4
Plant uptake
Plant N pools
Mortality & leaf fall
Litter N pools
Decomposition
Deep groundwater infiltration
Groundwater NO_3
Return flow
Infiltration
Infiltration
Soil NH_4
Nitrification
Mineralization
Immobilization
Soil NO_3
Soil organic N & soil microbe N pools
Surface runoff
Subsurface flow
Patch NO_3 export
Denitrification

Figure 3.

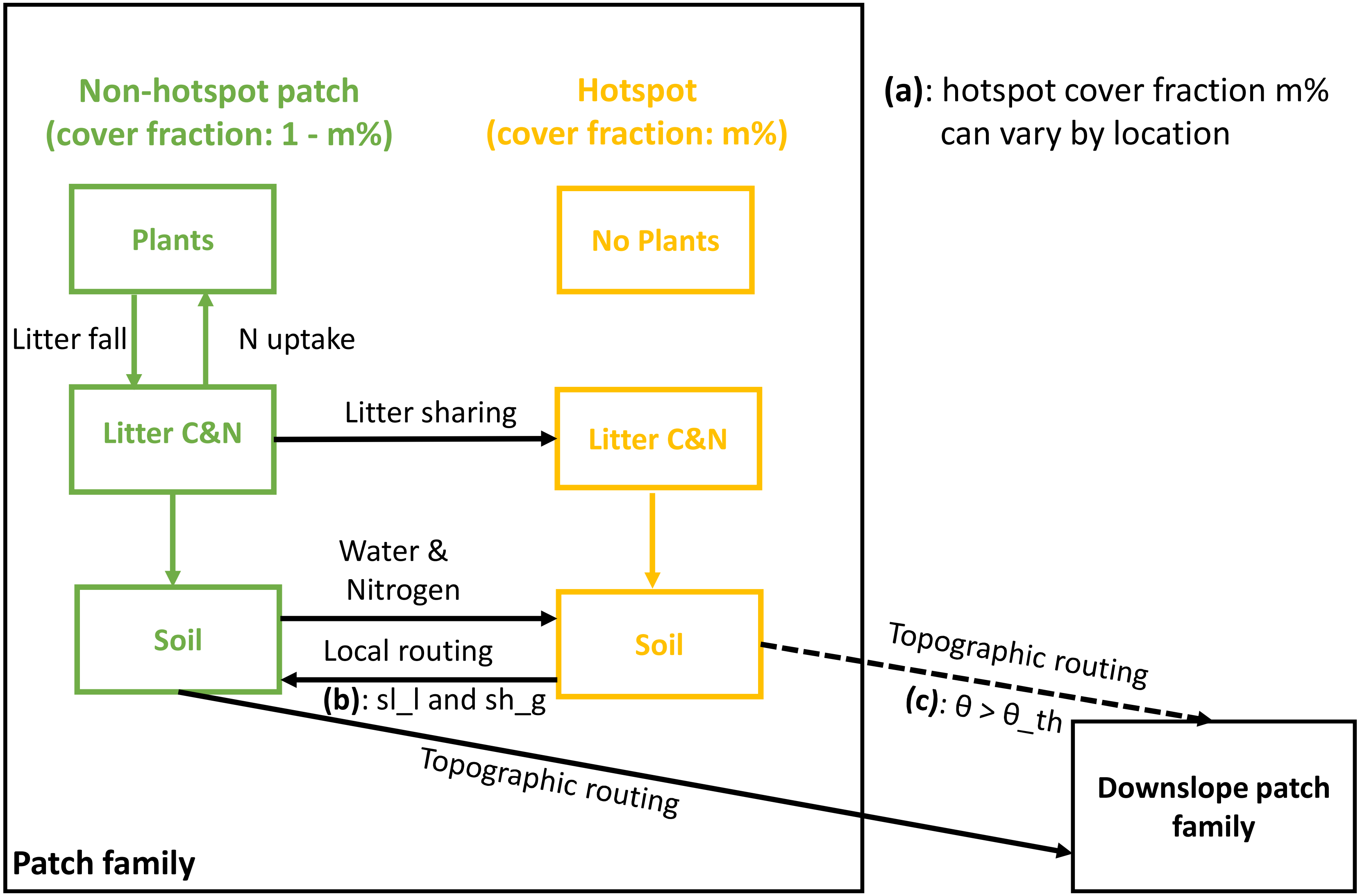
Non-hotspot patch
(cover fraction: 1 - m%)
Hotspot
(cover fraction: m%)
(a): hotspot cover fraction m%
can vary by location
Plants
No Plants
Litter fall
N uptake
Litter C&N
Litter sharing
Litter C&N
Water &
Nitrogen
Soil
Local routing
Soil
(b): sl_l and sh_g
Topographic routing
(c): θ > θ_th
Topographic routing
Downslope patch
family
Patch family

Figure 4.

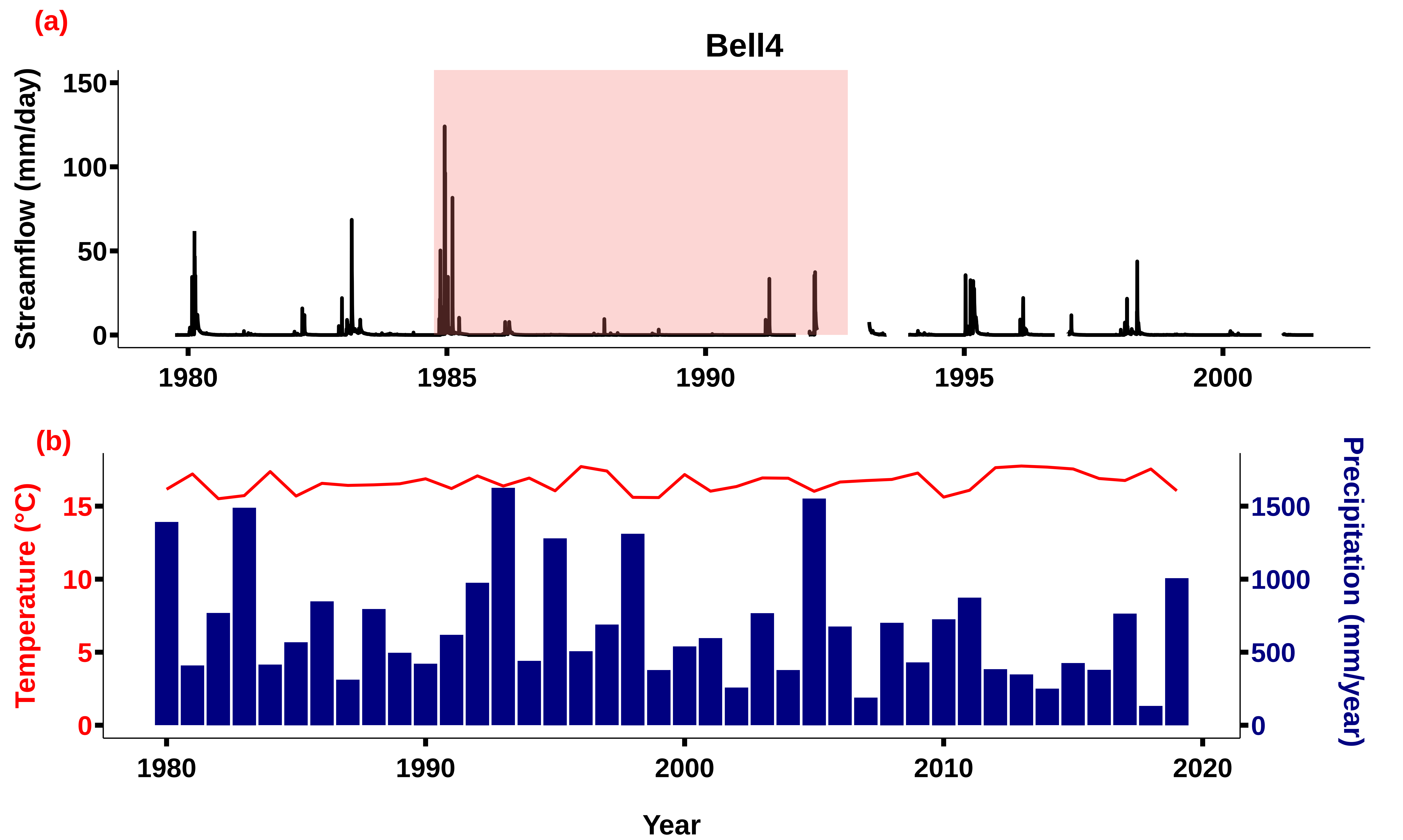
(a)
Bell4
Streamflow (mm/day)
0
50
100
150
1980
1985
1990
1995
2000
(b)
Temperature (°C)
0
5
10
15
Precipitation (mm/year)
0
500
1000
1500
1980
1990
2000
2010
2020
Year

Figure 5.

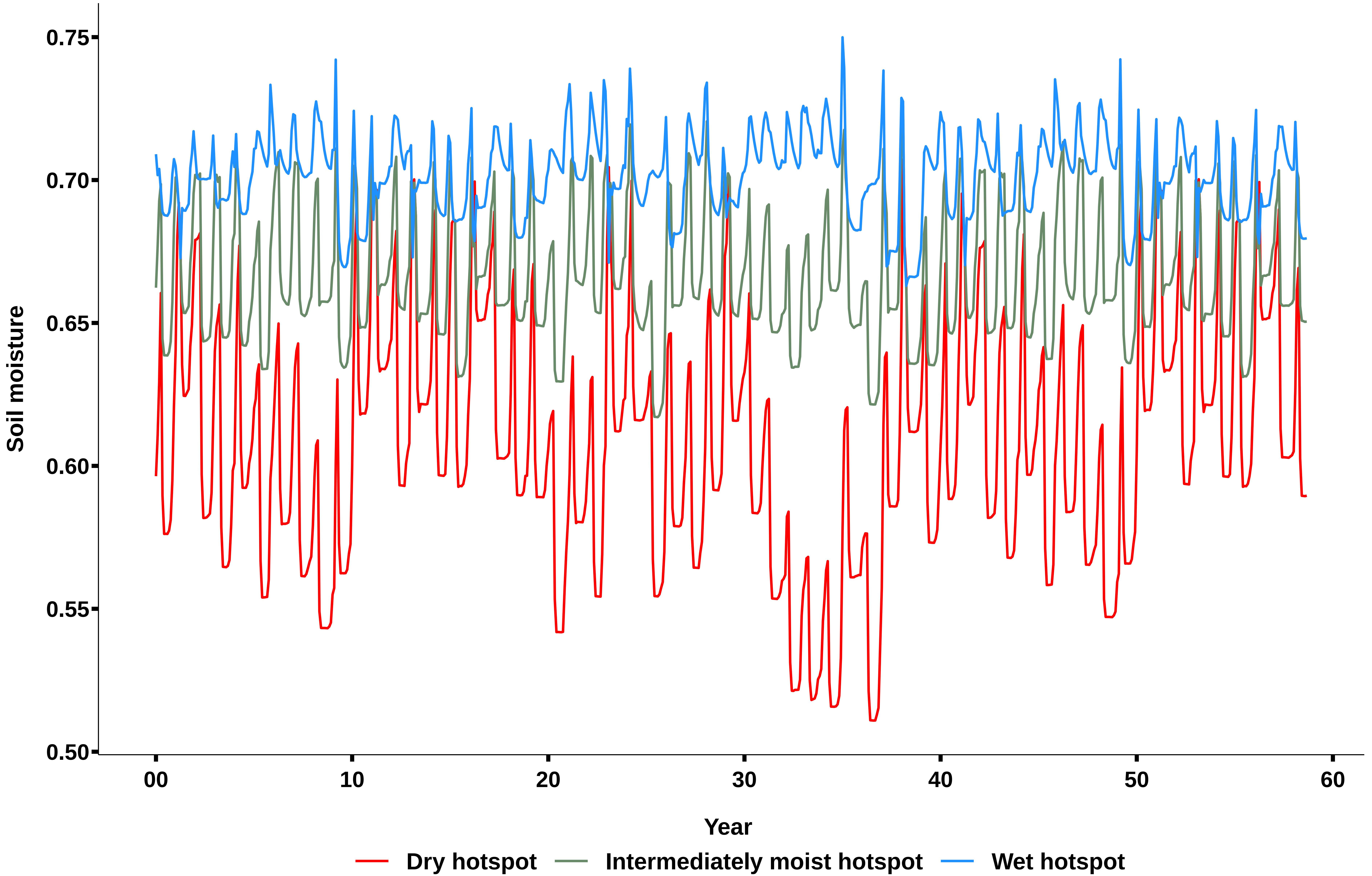

Soil moisture
0.75
0.70
0.65
0.60
0.55
0.50
00
10
20
30
40
50
60
Year
Dry hotspot
Intermediately moist hotspot
Wet hotspot

Figure 6.

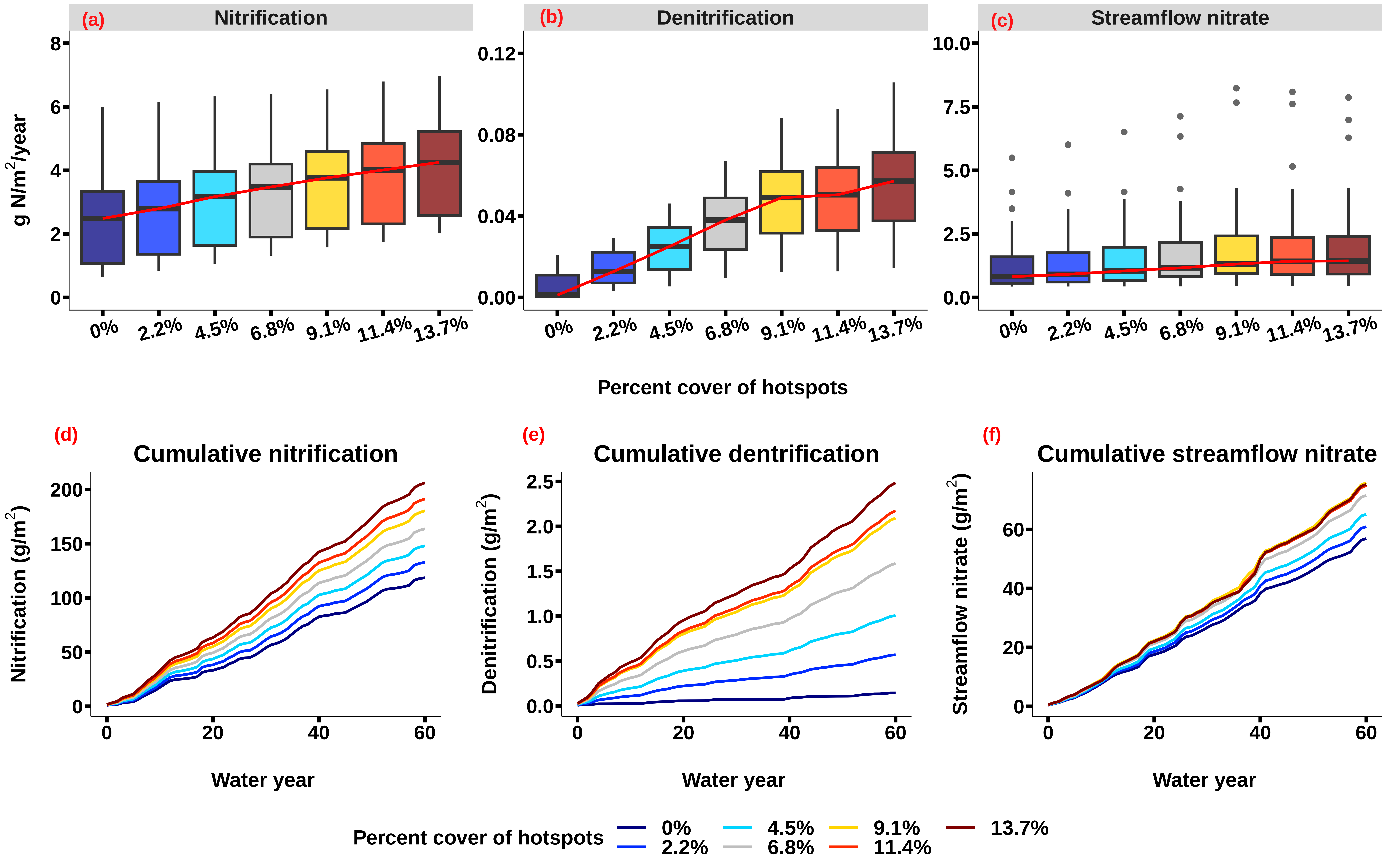

(a) Nitrification
(b) Denitrification
(c) Streamflow nitrate
g N/m^2/year
0%
2.2%
4.5%
6.8%
9.1%
11.4%
13.7%
Percent cover of hotspots
(d) Cumulative nitrification
(e) Cumulative dentrification
(f) Cumulative streamflow nitrate
Nitrification (g/m^2)
Denitrification (g/m^2)
Streamflow nitrate (g/m^2)
Water year
Percent cover of hotspots

Figure 7.

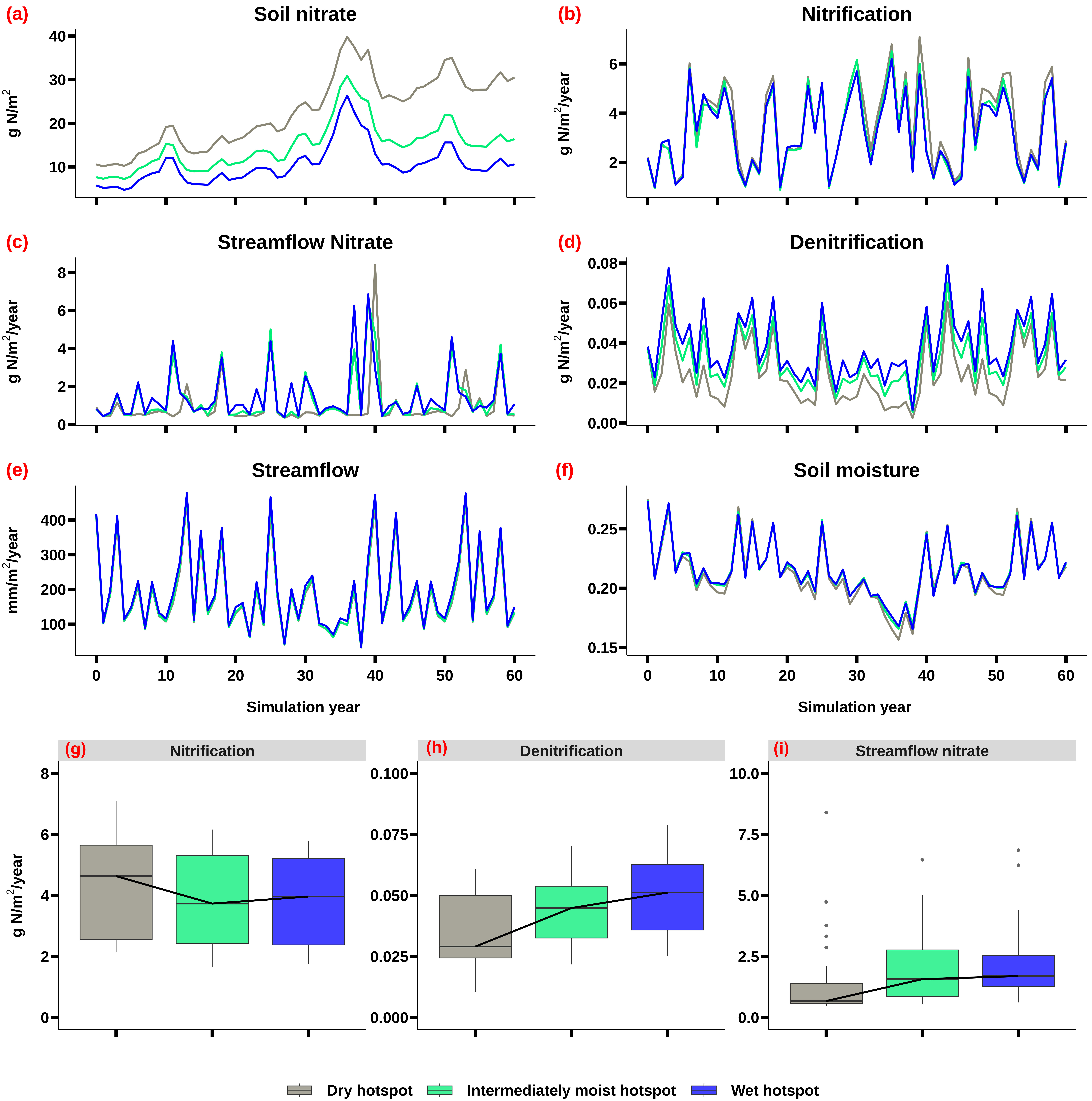

(a)
Soil nitrate
g N/m2
(b)
Nitrification
g N/m2/year
(c)
Streamflow Nitrate
g N/m2/year
(d)
Denitrification
g N/m2/year
(e)
Streamflow
mm/m2/year
(f)
Soil moisture
Simulation year
Simulation year
(g)
Nitrification
(h)
Denitrification
(i)
Streamflow nitrate
g N/m2/year
Dry hotspot
Intermediately moist hotspot
Wet hotspot

Figure 8.

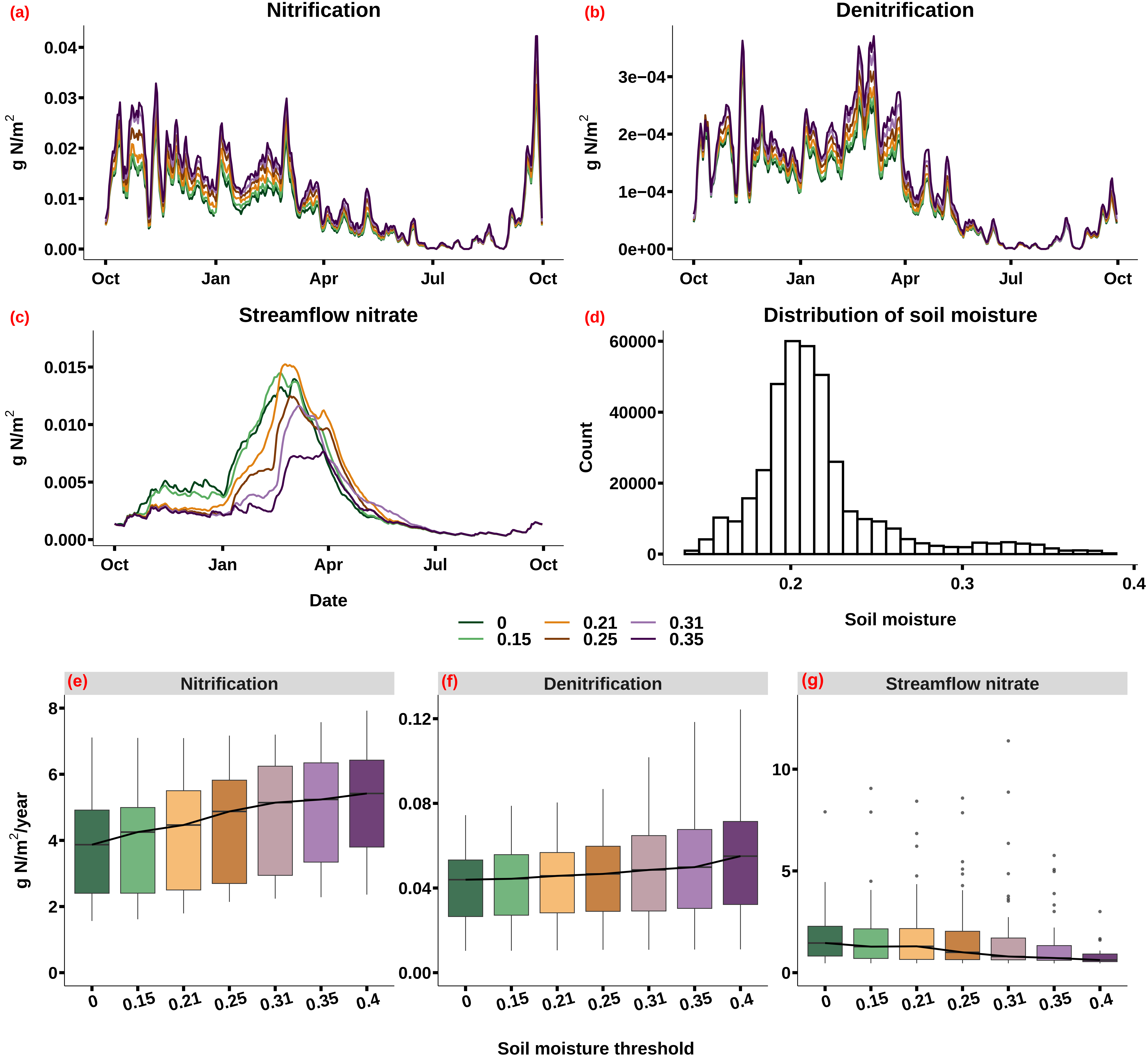
(a)
Nitrification
g N/m^2
0.00
0.01
0.02
0.03
0.04
Oct
Jan
Apr
Jul
Oct
(b)
Denitrification
g N/m^2
0e+00
1e−04
2e−04
3e−04
Oct
Jan
Apr
Jul
Oct
(c)
Streamflow nitrate
g N/m^2
0.000
0.005
0.010
0.015
Oct
Jan
Apr
Jul
Oct
Date
(d)
Distribution of soil moisture
Count
0
20000
40000
60000
0.2
0.3
0.4
Soil moisture
0
0.15
0.21
0.25
0.31
0.35
(e)
Nitrification
g N/m^2/year
0
2
4
6
8
(f)
Denitrification
0.00
0.04
0.08
0.12
(g)
Streamflow nitrate
0
5
10
0
0.15
0.21
0.25
0.31
0.35
0.4
Soil moisture threshold

Figure 9.

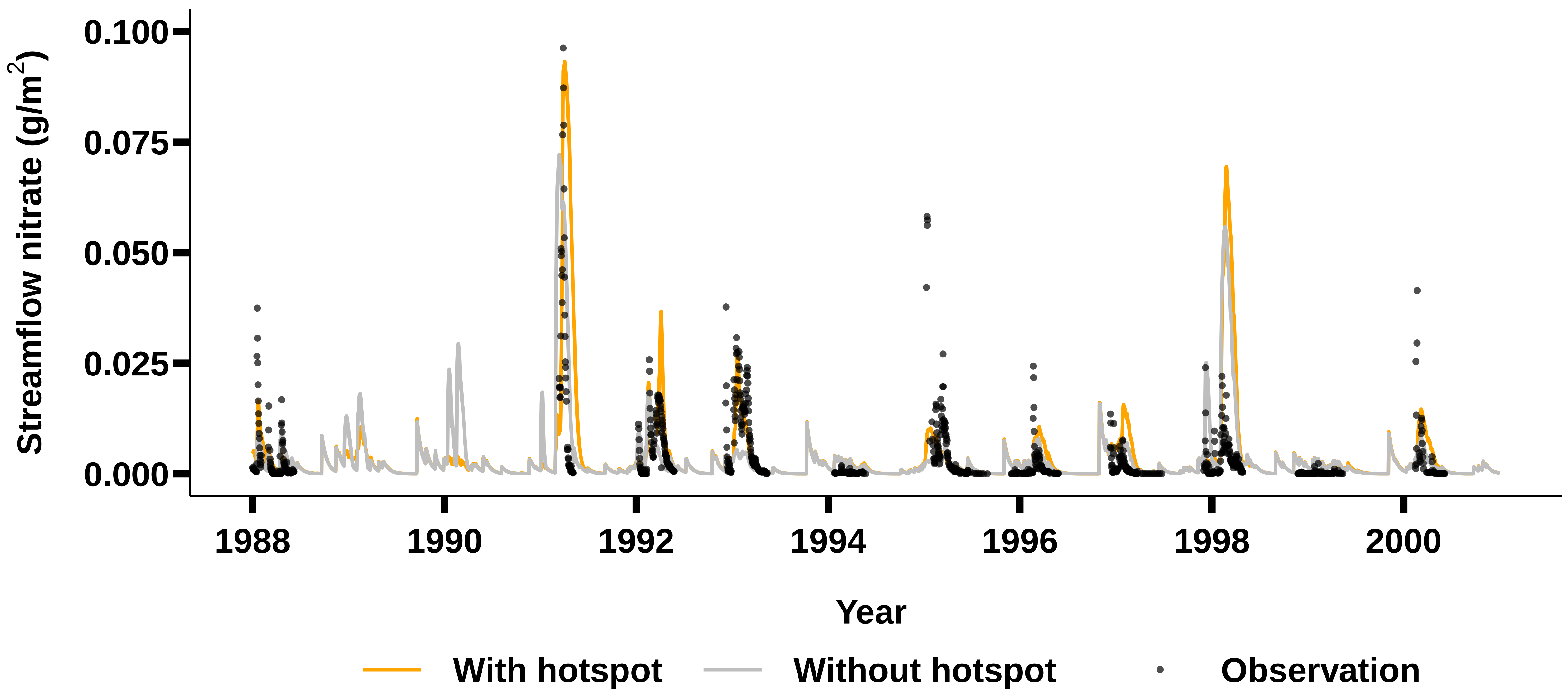

Streamflow nitrate (g/m^2)
0.100
0.075
0.050
0.025
0.000
1988
1990
1992
1994
1996
1998
2000
Year
With hotspot
Without hotspot
Observation

Figure 10.

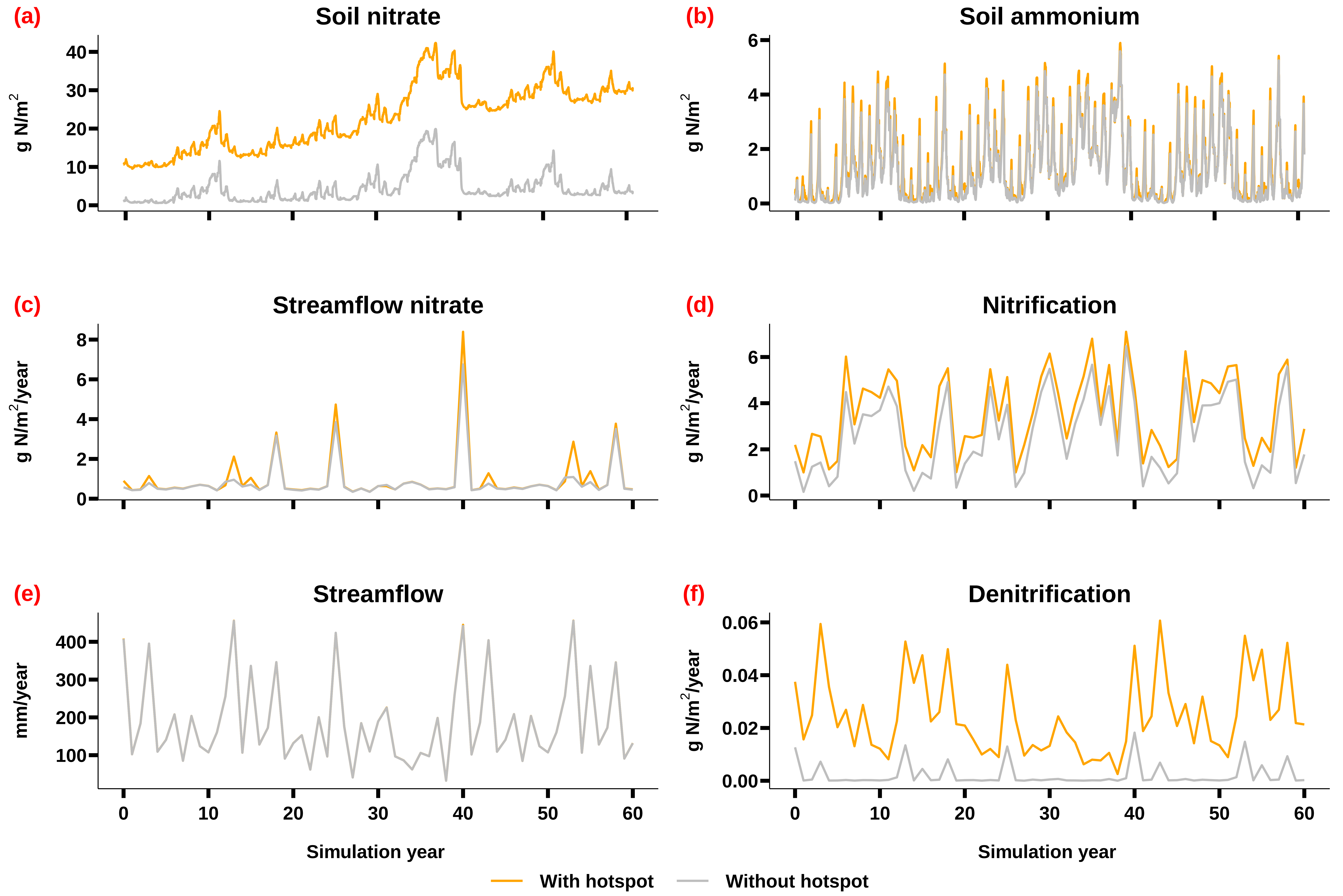
(a)
Soil nitrate
g N/m^2
(b)
Soil ammonium
g N/m^2
(c)
Streamflow nitrate
g N/m^2/year
(d)
Nitrification
g N/m^2/year
(e)
Streamflow
mm/year
(f)
Denitrification
g N/m^2/year
Simulation year
Simulation year
With hotspot
Without hotspot

Figure 11.

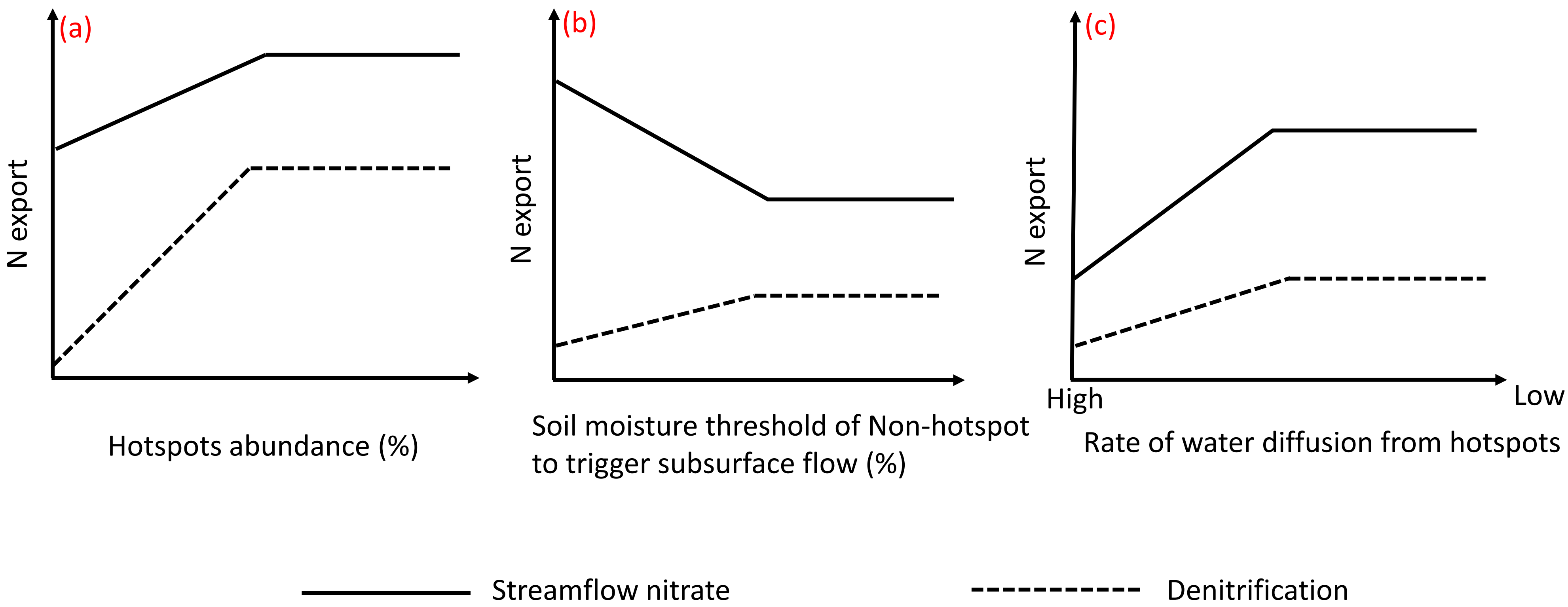

(a)
N export
Hotspots abundance (%)
(b)
N export
Soil moisture threshold of Non-hotspot
to trigger subsurface flow (%)
(c)
N export
High
Low
Rate of water diffusion from hotspots
Streamflow nitrate
Denitrification